IV. 研究成果の刊行物・別刷

Pharmaceutical Research, Vol. 27, No. 1, January 2010 (© 2009)
DOI: 10.1007/s11095-009-9987-y

Research Paper

Mathematical Model to Predict Skin Concentration of Drugs: Toward Utilization of Silicone Membrane to Predict Skin Concentration of Drugs as an Animal Testing Alternative

Kenji Sugibayashi,[1,2] Hiroaki Todo,[1] Takeshi Oshizaka,[1] and Yoko Owada[1]

Received June 5, 2009; accepted September 22, 2009; published online November 11, 2009

Purpose. To calculate the skin concentration of active ingredients in cosmetics and topical pharmaceuticals using silicone membrane permeation.
Methods. A series of parabens were used as model ingredients. Skin concentration of parabens was calculated using silicone membrane permeability. Their partition coefficient from formulations to the silicone membrane was determined by the membrane permeation profiles, and used to calculate their silicone membrane concentration, under an assumption that the membrane is one homogenous diffusion layer. The same procedure was applied for hairless rat skin.
Results. The calculated concentration of parabens in silicone membrane was very close to their observed values. However, the skin concentration calculated by skin permeability was not similar to the observed concentration. Re-calculation was performed under the assumption that the skin consists of two diffusion layers. This modification using permeation data through full-thickness and stripped skin enabled precise prediction of the skin concentration of parabens. In addition, the partition coefficient to the silicone membrane was useful to estimate their skin concentration.
Conclusions. Ingredient concentration in skin can be precisely predicted using diffusion equations and partition coefficients through permeation experiments using a silicone membrane. The calculated in-skin concentration is useful for formulation studies of cosmetics and topical pharmaceuticals.

KEY WORDS: hairless rat skin; membrane permeation; paraben; silicone membrane; skin concentration.

INTRODUCTION

Skin has been the focus as an application site of cosmetics and therapeutic drugs. Many transdermal drug delivery systems and topical drug formulations, as well as cosmetics, are on the market, and determining the percutaneous absorption of drugs and cosmetic ingredients is important for developing good topical formulations; however, percutaneous absorption or skin permeation itself is not always important for topical formulations (1). In other words, maintaining drug and active ingredient concentrations at their sites of action is more important for most topical drug and cosmetic formulations (2,3). For example, a lack of skin distribution and permeation are necessary for sunscreens, which mostly act on the skin surface, from a safety point of view. On the other hand, skin whitening agents must be studied for their skin distribution and concentration in the viable epidermis, which is their primary site of action. High skin permeation of whitening agents, however, is not expected, because the possibility of systemic side effects is increased. Of course, efficient percutaneous absorption or skin permeation of drugs is necessary for transdermal drug delivery systems to achieve systemic pharmacological actions. Thus, we have to distinguish the skin distribution or skin concentration from percutaneous absorption or skin permeation of drugs and cosmetic ingredients. This is very important to evaluating therapeutic drug formulations and cosmetics.

Unfortunately, little investigation has been performed of the skin distribution or skin concentration of chemical compounds compared with percutaneous absorption and skin permeation, especially for cosmetics. Epidermal layers frequently serve as a site of action for ingredients in cosmetics and topical drug formulations. Active ingredients and drugs in the formulations must distribute from the formulations to the epidermal tissues and maintain efficient concentrations in the tissues to achieve their effectiveness as cosmetics or topical drug formulations. In addition, the determination of skin concentration is very important for evaluating cosmetics or topical drug formulations, as well as for developing new cosmetic and drug products.

Recently, criticism against animal experiments has greatly increased from the viewpoint of animal welfare. In the EU, animal experiments to the production and import of cosmetic formulations are banned from 2009 to 2013 (4–7). Scientists have to be aware of the spirit of the 3Rs for animal

[1] Faculty of Pharmaceutical Sciences, Josai University, 1-1 Keyakidai, Sakado, Saitama 350-0295, Japan.
[2] To whom correspondence should be addressed. (e-mail: sugib@josai.ac.jp)

experiments: "Reduction" refers to methods that enable researchers to obtain comparable levels of information from fewer animals or to obtain more information from the same number of animals; "Refinement" refers to methods that alleviate or minimize potential pain, suffering or distress, and enhance the welfare of the animals used; and "Replacement" refers to the preferred use of non-animal methods over animal methods whenever it is possible to achieve the same scientific aims.

We therefore used silicone membrane as an alternative to skin membrane to determine the skin concentration of cosmetic ingredients or drugs, from the viewpoints of the great necessity of estimating their concentration in the skin in the development of cosmetics or topical formulations, and as an animal experiment alternative. Silicone membrane has been used as an alternative to skin membrane, and the permeation of cosmetic ingredients and drugs through the silicone membranes was compared with that through human or animal skin (8–11). Few experiments have been performed, however, on their skin or membrane concentration. In the present study, a method for estimating skin concentration was established using silicone membrane permeability. A series of parabens (methyl, ethyl, *n*-propyl, *n*-butyl esters) were used as model penetrants, since they have very different lipophilicities (*i.e.*, n-octanol/water partition coefficient) in spite of having a similar molecular weight (152–194 Da). Table I summarizes the physicochemical properties of parabens used in this experiment (12).

THEORETICAL (13,14)

One-Layered Diffusion Model (15)

Determination of Membrane Concentration

The diffusion of chemical compounds in the membrane is expressed theoretically by Fick's second law of diffusion, $\frac{\partial C}{\partial t} = D\frac{\partial^2 C}{\partial x^2}$, under the assumption that the membrane is a homogeneous single layer, where C is the penetrant concentration in the membrane at position, x, and time, t. When a sink condition is assumed on the receiver side of the membrane, *i.e.*, x = L, a set of initial conditions (C=0 at t=0 and 0<x<L)) and boundary conditions (C = KC_v at x=0 and C=0 at $x = L$, where K is the partition coefficient of the penetrant from the vehicle to membrane and C_v is the penetrant concentration in the vehicle) are obtained (see Fig. 1a).

Then, membrane concentration, C, and its steady-state level at an infinite time, C_{ss}, are expressed as follows (12):

$$C = KC_v\left\{\left(1-\frac{x}{L}\right) - \frac{2}{\pi^2}\sum_{n=1}^{\infty}\sin\frac{nx\pi}{L}\exp\left(-\frac{Dn^2\pi^2}{L^2}t\right)\right\} \quad (1)$$

$$C_{ss} = KC_v\left(1-\frac{x}{L}\right) \quad (2)$$

Further, the mean membrane concentrations of penetrant, $\overline{C}$ and $\overline{C}_{ss}$, are obtained by integrating C in Eqs. 1and 2 from x=0 to L:

$$\overline{C} = \frac{KC_v}{2}\left\{1 - \frac{8}{\pi^2}\sum_{m=1}^{\infty}\frac{1}{(2m-1)^2}\exp\left(-\frac{D(2m-1)^2\pi^2}{L^2}t\right)\right\} \quad (3)$$

$$\overline{C}_{ss} = \frac{KC_v}{2} \quad (4)$$

As shown in Eq. 4, the mean membrane concentration of the penetrant can be determined by K and C_v, not by D. Because C_v is a known parameter, a parameter, K, is the only determinant of the mean membrane concentration of the penetrant.

Determination of Membrane Permeation

Since the silicone membrane can be supposed to be homogenous in one layer, the permeation profiles of parabens throughout the membrane were analyzed using a one-layered diffusion model (16,17). Under the initial and boundary conditions shown above, the amount of drug permeating the unit area of the silicone membrane at time t, Q, can be represented as

$$Q = KLC_v\left[\frac{D}{L^2}t - \frac{1}{6} - \frac{2}{\pi^2}\sum_{n=1}^{\infty}\frac{(-1)^n}{n^2}\exp\left(-\frac{D}{L^2}n^2\pi^2 t\right)\right] \quad (5)$$

The partition parameter ($K{\cdot}L$) and diffusion parameter (D/L^2) were obtained by curve fitting the obtained data to Eq. 5 using the least squares method. In the calculation of D and K, the thickness of the silicone membrane was fixed at 68 μm. Permeability coefficient, P, was calculated by an equation, $P = \frac{KD}{L}$.

Table I. Physicochemical Parameters of Parabens

	Methyl paraben (MP)	Ethyl paraben (EP)	Propyl paraben (PP)	Butyl paraben (BP)
M.W.	152.12	166.18	180.20	194.23
Log K_{ow} [a)]	0.940	1.93	2.27	3.53
clog P [b)]	1.98	2.51	3.04	3.57
Solubility[c)](mM)	19.7	8.82	2.27	1.60

[a)] *n*-Octanol / water partition coefficient at 37°C
[b)] Calculation by software, Chem Draw (CambridgeSoft)
[c)] In water at 32°C

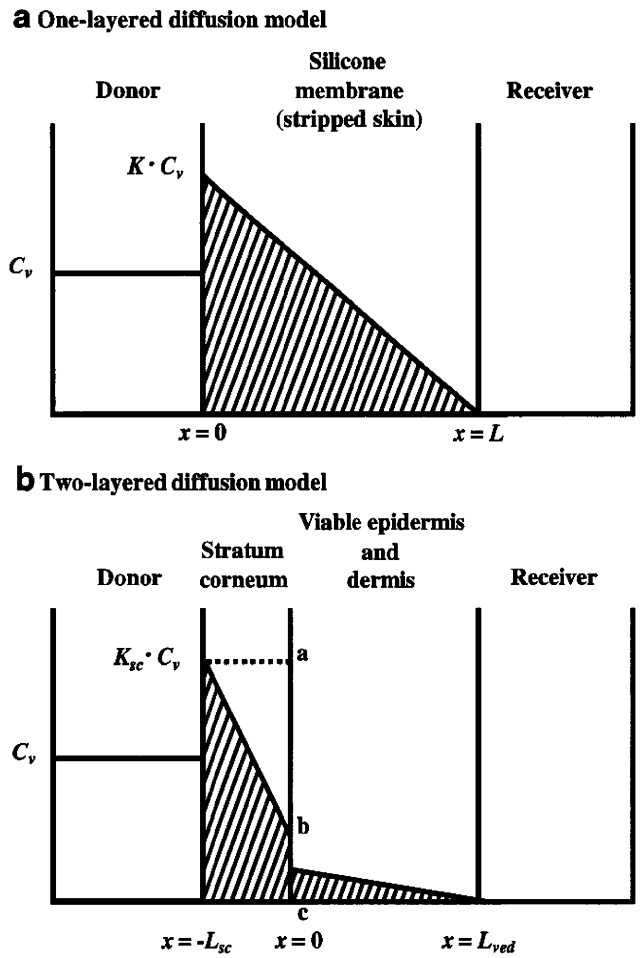

Fig. 1. Schematic diagram of concentration-distance profile in one- and two-layered diffusion membrane models in membrane permeation experiments. Membrane thickness is L and $L_{sc}+L_{ved}$ for one- and two-layered diffusion membranes models, respectively. C_v is the donor concentration of parabens, and K and K_{sc} are partition coefficients to membranes.

Stripped hairless rat skin was treated as a homogeneous layer, the same as the silicone membrane.

Two-Layered Diffusion Model

Determination of Membrane Concentration Using Two-Layered Diffusion Model

Fig. 1b shows a typical two-layered diffusion model of skin. Penetrant concentration in the first layer of skin, the stratum corneum, C_{sc}, and that in the second layer, the viable epidermis and dermis of skin, C_{ved}, can be expressed by Fick's second law of diffusion. Similarly, initial conditions and boundary conditions are represented. Boundary condition between the first and second layer is $C_{ved} = K_{sc}K_{ved}C_{sc}$ and $D_{sc}\frac{dCsc}{dx} = D_{ved}\frac{dCved}{dx}$, where K_{sc} and K_{ved} are partition coefficients of the penetrant from the vehicle to stratum corneum and to the viable epidermis and dermis, and D_{sc} and D_{ved} are diffusion coefficients in the stratum corneum and viable epidermis and dermis, respectively.

In the two-layered diffusion model, the overall permeability coefficient, P_{tot}, can be expressed by that in the stratum corneum, P_{sc}, and in the viable epidermis and dermis, P_{ved}, as follows, in Eq. 6. (18):

$$\frac{1}{P_{tot}} = \frac{1}{P_{sc}} + \frac{1}{P_{ved}} \tag{6}$$

In addition, the reciprocal of the permeability coefficient can be replaced with permeation resistant, R, and the following equation can be derived, as Eq. 7:

$$R_{tot} = R_{sc} + R_{ved} \tag{7}$$

The permeation resistance of the penetrants can be represented as in the electric circuit. Two resistances, R_{sc} and R_{ved}, exist in the skin membrane, as shown in Fig. 1b. The ratio of the Line segment ab against bc at the surface between the stratum corneum and viable epidermis, x=0, should be the ratio of R_{sc} against R_{ved}. Thus, the penetrant concentration at point b, C_b, can be represented by

$$C_b = K_{sc}C_v\frac{R_{ved}}{R_{tot}} \tag{8}$$

The amount of penetrant in the unit area of the stratum corneum, M_{sc}, can be represented using Eq. 8 as Eq. 9.

$$M_{sc} = \frac{K_{sc}C_vL_{sc}\left(1+\frac{R_{ved}}{R_{tot}}\right)}{2} \tag{9}$$

Since the partition coefficient of the penetrant from the stratum corneum to the viable epidermis and dermis is represented as K_{ved}/K_{sc}, the amount of penetrant in the unit area of the viable epidermis and dermis, M_{ved}, can be represented as

$$M_{ved} = \frac{K_{ved}C_vL_{ved}\frac{R_{ved}}{R_{tot}}}{2} \tag{10}$$

By summation of Eqs. 9 and 10, M_{tot}, the drug amount in the unit area of the skin can be represented as follows:

$$M_{tot} = \frac{C_v}{2}\left\{K_{sc}L_{sc}\left(1+\frac{R_{ved}}{R_{tot}}\right) + K_{ved}L_{ved}\frac{R_{ved}}{R_{tot}}\right\} \tag{11}$$

By dividing M_{tot} in Eq. 11 by skin thickness, L_{tot}, the average drug concentration in the skin, $\overline{C}_{ss}$, is

$$\overline{C}_{ss} = \frac{C_v}{2L_{tot}}\left\{K_{sc}L_{sc}\left(1+\frac{R_{ved}}{R_{tot}}\right) + K_{ved}L_{ved}\frac{R_{ved}}{R_{tot}}\right\} \tag{12}$$

When resistances, R, are changed to permeability coefficients, P, finally Eq. 13 is derived,

$$\overline{C}_{ss} = \frac{C_v}{2L_{tot}}\left\{K_{sc}L_{sc}\left(1+\frac{P_{tot}}{P_{ved}}\right) + K_{ved}L_{ved}\frac{P_{tot}}{P_{ved}}\right\} \tag{13}$$

Determination of Membrane Permeation Using Two-Layered Diffusion Model

Two diffusion coefficients, D_{sc} and D_{ved}, and two partition coefficients, K_{sc} and K_{ved}, were obtained by curve fitting the cumulative amount of parabens that permeated through the full-thickness skin and stripped skin to the

theoretical values using the least squares method, where theoretical values were expressed by two diffusion equations (Fick's second law) showing the diffusion profiles in the stratum corneum and viable epidermis and dermis. Differential equations describing Fick's second law are as follows (14):

$$\frac{dC_{i,j}}{dt} = \frac{1}{\Delta t}(C_{i,j+1} - C_{i,j}) \quad (14)$$

$$\frac{d^2C_{i,j}}{dx^2} = \frac{1}{\Delta x^2}(C_{i-1,j} - 2C_{i,j} + C_{i+1,j}) \quad (15)$$

Mathematical treatment for determining the skin permeation using two-layered diffusion model was the same as in our previous method (14).

Calculation of Permeation Parameters

Generally, most resistance against drug permeation throughout hairless rat skin is in the stratum corneum (17). Rat skin was also treated as a single-layered membrane, the same as the silicone membrane. Parameters D and K were calculated under the assumption that the stratum corneum is a homogeneous membrane with a thickness of 15μm.

Calculation of Theoretical Membrane Concentration of Parabens

The theoretical membrane concentration of parabens was calculated by Eq. 6 and the K value obtained from the membrane permeation study.

EXPERIMENT

Reagents and Materials

Parabens: methyl paraben (MP), ethyl paraben (EP), *n*-propyl paraben (PP), and *n*-butyl paraben (BP) were obtained from Tokyo Kasei Chemical Co., Ltd. (Tokyo, Japan). An esterase inhibitor, diisopropyl fluorophosphate (DFP), and a deproteinization agent, trichloroacetic acid (TCA), were obtained from Wako Pure Chemical Industries, Ltd. (Osaka, Japan). Other reagents and solvents were liquid chromatograph and special grade chemicals.

The silicone membrane (Dow Corning 7-4107) was a gift from Nagase & Co., Ltd. (Tokyo, Japan).

Experimental Animals

Male hairless rats (WBM/ILA-Ht, 230–280 g) were obtained from the Life Science Research Center, Josai University (Sakado, Saitama, Japan) or Ishikawa Experimental Animal Laboratories (Fukaya, Saitama, Japan). All animal experiments were performed according to the ethics committee of Josai University.

Membrane Permeation Experiments of Parabens

The silicone membrane was set on a Franz-type diffusion cell (receiver cell volume: 6.0 mL, effective diffusion area: 1.77 cm^2) using cyanoacrylate glue (19–22). Phosphate-buffered saline (pH 7.4, PBS) was applied to the receiver cell and maintained at 32°C for 15 min. Aliquots (0.5 mL) of different concentrations of parabens (MP 10 mM, EP 5 mM, PP 1 mM, BP 0.5 mM) in PBS were applied to the donor cell to start the permeation experiment. The experimental setup is shown in Fig. 2. The receiver solution was stirred on a magnetic stirrer with a bar; the experiment was performed at 32°C. At predetermined intervals, 400μL of the receiver solution was sampled, and the same volume of PBS was added to the receiver cell to keep the volume constant. Paraben concentration was determined by HPLC.

Abdominal skin (full-thickness skin or stripped skin) was excised from hairless rats under pentobarbital (25 mg/kg, *i.p.*) anesthesia, and debris and excess fat were trimmed off the excised skin. Stripped skin was made by tape-stripping the stratum corneum 20 times before excising from rats (23). The obtained skin piece was then set on the Franz-type diffusion cell, as above. DFP (2.7μmol/mL in PBS) was applied to the receiver cell for half an hour (12,24–26). After rinsing off the reagent, paraben solution (0.5 mL) in PBS and DFP in PBS (0.54μmol/mL, 6.0 mL) were added to the donor and receiver cells, respectively, to start the skin permeation experiment. Other procedures were consistent with the silicone membrane permeation experiments.

Determination of Extraction Ratio of Parabens

Silicone Membrane. Silicone membrane was loaded with parabens in chloroform and dried. Fresh chloroform (1 mL) was then applied to the silicone membrane piece. After agitating for 15 min, the resulting chloroform was sampled, and fresh chloroform was again added for the second extraction of parabens. Total chloroform containing parabens was evaporated to dryness, and the sample was reconstituted with 1.0 mL acetonitrile. The sample was injected onto HPLC to determine the paraben concentration. The extraction ratio of parabens from silicone membrane was almost 1.0.

Hairless Rat Skin. Hairless rat skin was loaded with parabens in water, and the skin piece was minced with scissors and homogenized at 12,000 rpm using a homogenizer (Polytron PT-MR 3000; Kinematica Inc., Littau, Switzerland) for 5 min at 4°C. The homogenate was incubated for 1 h at 32°C. The same volume of 16% TCA was added to the skin homogenate and agitated for 15 min (27–29). The supernatant after centrifugation (15,000 rpm, 5 min, 4°C) was injected onto HPLC. Parabens were extracted from the skin homogenate using chloroform, as in the silicone membrane experiment. The extraction ratio of parabens was almost 1.0.

Determination of Paraben Concentration in Silicone Membrane and Hairless Rat Skin

Silicone Membrane. After the permeation experiment, the donor solution was removed, and the silicone membrane was washed with PBS (1 mL). Chloroform (1 mL) was added to the silicone membrane in the Franz-type diffusion cell (permeation area: 1.77 cm^2) and agitated for 15 min to extract parabens from the membrane. The subsequent procedure was consistent with Determination of Extraction Ratio of Parabens.

Hairless Rat Skin. After the permeation experiment, the donor solution was removed, and the stratum corneum side

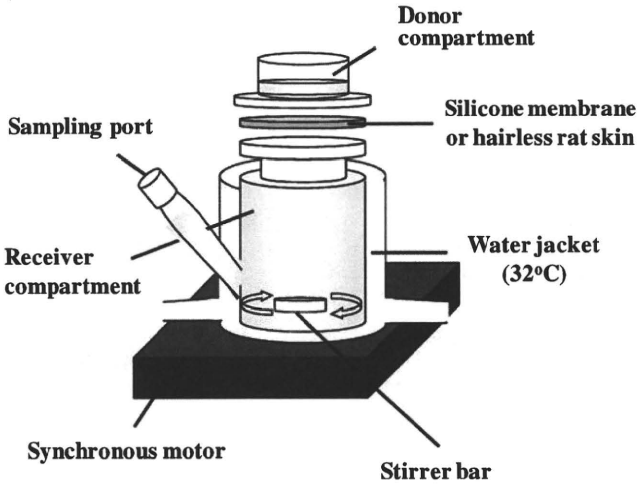

Fig. 2. Schematic representation of permeation experiment using silicone membrane and hairless rat skin.

of hairless rat skin was washed two times with PBS (1 mL). The rat skin was taken from the diffusion cell, and the permeation area of the skin (1.77 cm^2) was kept in a freezer (-15°C) before determining the skin concentration. This frozen skin was minced with scissors, and PBS (1 mL) was added to homogenize the minced skin (12,000 rpm, 5 min, 4°C). The subsequent procedure was consistent with Determination of Extraction Ratio of Parabens.

Determination Methods of Parabens

The same volume of acetonitrile containing an internal standard (another paraben) was added to the paraben samples. After slight mixing, the sample was injected onto HPLC. The HPLC system consists of a pump (LC-10 AD; Shimadzu, Kyoto, Japan), Chromatopac (C-R6A; Shimadzu), UV detector (SPD-6A; Shimadzu), system controller (SCL-6B; Shimadzu) and an auto-injector (SIL-7A; Shimadzu). The column was LiChroCART®250-4 (KGaA·64271; Merck, Darmstadt, Germany) kept at 40°C during the eluting mobile phase, 0.1% phosphoric acid : acetonitrile=75 : 25 for MP and EP and 0.1% phosphoric acid : acetonitrile=55 : 45 for PP and BP. The flow rate was 1.0 mL/min. The injection volume was 20μL, and detection was performed at 260 nm.

RESULTS AND DISCUSSIONS

Partition Coefficient and Concentration of Parabens into and in the Silicone Membrane

Since drug distribution in the skin membrane is a physical phenomenon, it can be evaluated using artificial membranes as well as human and animal skin. A silicone membrane was used in this experiment due to its cost and easy availability.

The direct measurement of drug concentration in the membrane has several problems. Generally, only one data point is obtained from one membrane after drug application. In addition, controlling the removal of the drug formulation from the membrane surface is very difficult. Hard cleaning of

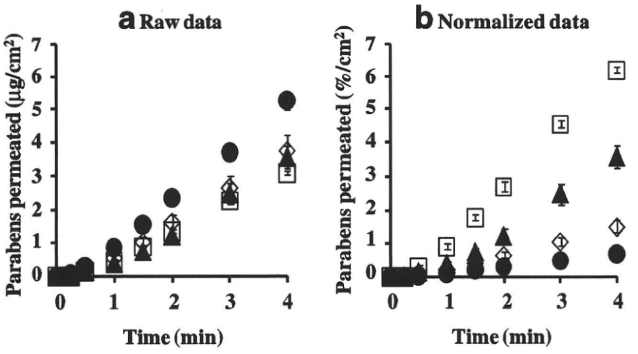

Fig. 3. Time course of the cumulative amount of parabens that permeated the silicone membrane. (**a**) raw data, (**b**) normalized data. Symbols: ●: 10 mM MP, ◊: 5 mM EP, ▲: 1 mM PP, □: 0.5 mM BP. Each data point represents the mean±S.E. (n=4–8).

the membrane surface decreases the membrane concentration, whereas inadequate cleaning may leave the drug formulation on the membrane. We first performed the membrane permeation experiment, and permeation parameters were obtained. The membrane concentration can be calculated using the partition coefficient, K, of the applied drug from the vehicle to the membrane, as shown in Eq. 6. Next, the calculated values were compared with the directly observed membrane concentration. The membrane was obtained after the membrane permeation experiments.

Fig. 3 shows the cumulative amount of parabens that permeated the silicone membrane. Fig. 3a and b show raw and normalized data (raw data divided by application concentration of parabens (19,30)), respectively. The permeation ratio of BP against the application amount was highest, followed by PP, EP and MP. The increase in the lipophilicity of parabens increased the permeability, as shown in Fig. 3b (31).

Generally, high permeability and solubility of chemicals through and in the membrane are observed when the solubility parameter of chemicals is close to that of membrane. The solubility parameter of BP, 10.9 $(cal/cm^3)^{1/2}$, is closest to that of the silicone membrane (7.3–7.5 $(cal/cm^3)^{1/2}$) among the parabens (MP: 11.5 $(cal/cm^3)^{1/2}$, EP: 11.3 $(cal/cm^3)^{1/2}$, PP: 11.1 $(cal/cm^3)^{1/2}$) used in this experiment (32–34).

Fig. 4a and b show the observed concentration and normalized concentration corrected using the application concentration of parabens in the silicone membrane, respectively. Each concentration is that at the steady state after

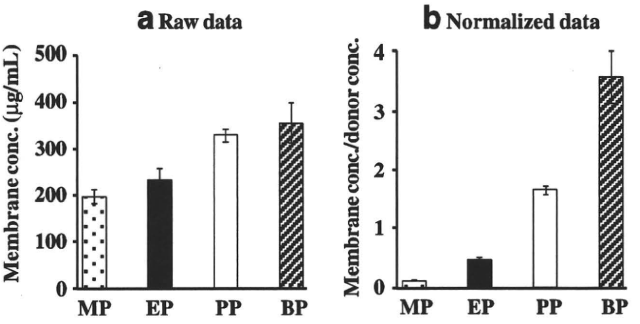

Fig. 4. Raw data (**a**) and normalized date [(silicone membrane concentration)/(donor concentration)] (**b**) for steady-state silicone membrane concentration of parabens. Each column represents the mean ± S.E. (n=4–8).

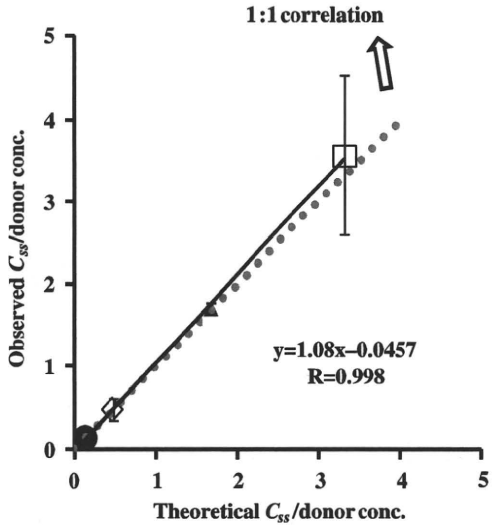

Fig. 5. Relationship between theoretical and observed steady-state silicone membrane concentration of parabens. Normalized data were used (see Fig. 4). One-layered diffusion membrane model was used to obtain theoretical steady-state membrane concentration of parabens. Symbols: see Fig. 3. The observed data represent the mean ± S.D. (n=4–8). Almost 1:1 correlation was found. K, D and P were as follows (D :$\times 10^{-7}$cm^2/s, P :$\times 10^{-5}$cm/s): MP (K=0.256, D=4.07, P=1.53), EP (K=0.907, D=2.60, P=3.47), PP (K=3.34, D=1.78, P=8.76), and BP (K=6.64, D=1.65, P=16.1).

starting the permeation experiments. An increase in $K_{o/w}$ of parabens increases the membrane concentration.

Fig. 5 shows the relationship between the theoretical and observed values of paraben concentration in the silicone membrane. This figure shows almost a 1:1 relationship between them, suggesting that the silicone membrane can be assumed to be one homogenous layer and that the membrane concentration of parabens can be theoretically determined by C_v and K. These results also suggest that the permeation experiment is useful to determine the membrane concentration. The figure also contains the permeation parameters of parabens in the legend. The permeation parameters were obtained by curve-fitting the permeation profiles to Fick's law of diffusion using the nonlinear least squares method, under the assumption that the silicone membrane is one homogenous layer. The permeability coefficient, P, of MP and BP was lowest and highest among the parabens used in this experiment. The diffusion coefficient, D,

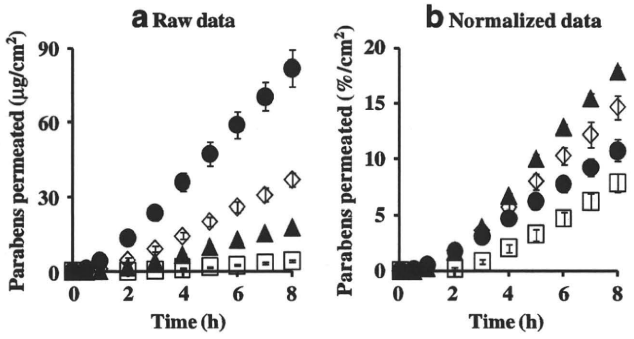

Fig. 6. Time course of the cumulative amount of parabens that permeated hairless rat intact skin. (**a**) raw data, (**b**) normalized data Symbols: see Fig. 3. Each data point represents the mean ± S.E. (n=5–11).

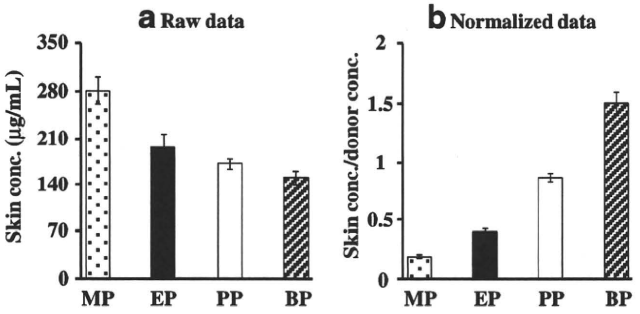

Fig. 7. Raw data (a) and normalized date [(skin concentration)/(donor concentration)] for steady-state hairless rat skin concentration of parabens. Each column represents the mean ± S.E. (n=5–11).

of these parabens in the silicone membranes was not so different (only 2–3 times different), whereas partition coefficient, K, was very different among these parabens (26 times different between MP and BP). A very different permeability coefficient, P, is closely related to the K of parabens. Since the P-value of parabens throughout the silicone membrane was very high (about 10^{-5}cm/s), the permeation profiles can be evaluated in a short experimental period. The theoretical membrane concentration of parabens calculated from the K-value was very close to the observed membrane concentration.

Membrane Permeation and Concentration: Comparison Between Silicone Membrane and Animal Skin

The theoretical concentration of parabens in silicone membrane, which was calculated from partition coefficient, K, was close to the observed concentration. A similar trial was carried out for the paraben concentration in hairless rat skin. Partition and skin concentration of parabens in rat skin were compared to those in the silicone membrane.

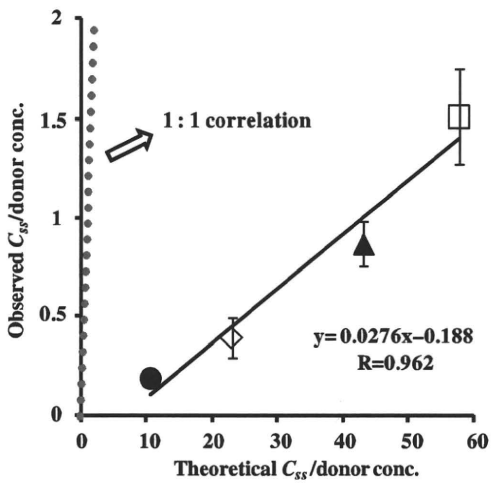

Fig. 8. Relationship between theoretical and observed steady-state hairless rat skin concentration of parabens. Normalized data were used (see Fig. 7). One-layered diffusion membrane model was used to obtain theoretical steady-state membrane concentration of parabens. Symbols: see Fig. 3. The observed data represent the mean ± S.D. (n=5–11). The obtained line was very different from 1:1 correlation. K, D and P were as follows (D :$\times 10^{-11}$cm^2/s, P :$\times 10^{-6}$cm/s): MP (K=21.3, D=14.2, P=2.03), EP (K=46.1, D=10.2, P=3.15), PP (K=86.3, D=6.67, P=3.84), and BP (K=115, D=1.63, P=1.26).

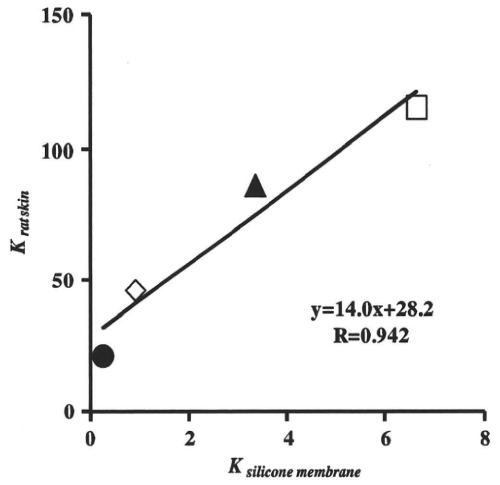

Fig. 9. Relationship between K to silicone membrane and K to rat skin (one-layered diffusion model). Symbols: see Fig. 3. Each data point represents the mean ± S.E. (n=4–8 in silicone membrane data and 5–11 in rat skin data).

Fig. 6 shows the cumulative amount of parabens that permeated the excised hairless rat skin. Fig. 6a and b show the mean raw data and normalized permeation data. The latter was normalized by the application amount of parabens. The raw skin permeation data of parabens, as shown in Fig. 6a, are similar to silicone membrane permeation; however, the permeability coefficient ratio of BP against MP in hairless rat skin was much larger than that in the silicone membrane. This may have been due to the different permeation pathways between the silicone membrane and rat skin. The silicone membrane is a homogeneous membrane, whereas hairless rat skin has appendages, such as hair follicles, as well as the stratum corneum pathway. Interestingly, BP permeation through the silicone membrane was highest in the normalized data (Fig. 3b) among the parabens used in the present study, whereas PP permeation through rat skin was highest (Fig. 6b). These data are probably due to similar solubility parameter of BP or PP to that of the silicone membrane or rat skin, respectively.

Fig. 7a and b show the observed and normalized concentrations of parabens corrected using their application concentrations in hairless rat skin, respectively. Each paraben concentration in rat skin was that at the steady state after

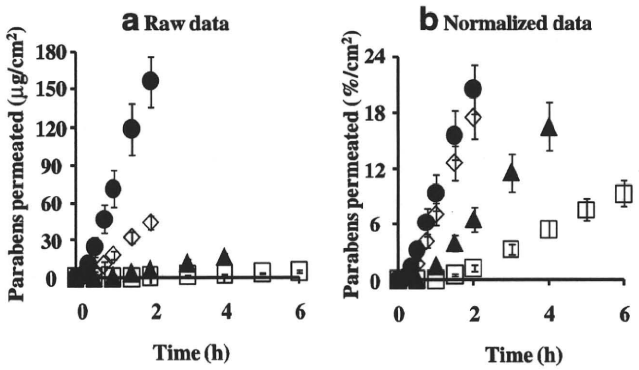

Fig. 10. Time course of the cumulative amount of parabens that permeated hairless rat stripped skin. (**a**) raw data, (**b**) normalized data. Symbols: see Fig. 3. Each data point represents the mean ± S.E. (n=3).

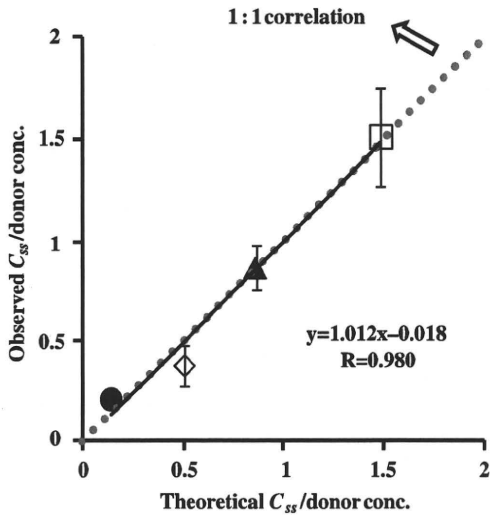

Fig. 11. Relationship between theoretical and observed C_{ss} in hairless rat skin. Normalized data were used (see Fig. 7). Two-layered diffusion membrane model was used to obtain theoretical steady-state skin concentration of parabens. Symbols: see Fig. 3. The observed data represent the mean±S.D. (n=3–8). Almost 1:1 correlation was found. K, D and P were as follows (D_{sc} :× 10^{-10}cm^2/s, P_{tot} :×10^{-6}cm/s, D_{ved} :×10^{-7}cm^2/s, P_{ved} :×10^{-5}cm/s): MP (K_{sc}=4.55, D_{sc}=9.38, P_{tot}=2.46, K_{ved}=2.95, D_{ved}=3.66, P_{ved}= 1.85), EP (K_{sc}=9.18, D_{sc} = 9.36, P_{tot}=5.73, K_{ved}=5.23, D_{ved}=2.19, P_{ved}=1.96), PP (K_{sc}=48.6, D_{sc}=5.72, P_{tot}=0.859, K_{ved}=2.57, D_{ved}= 1.78, P_{ved}=0.628), and BP (K_{sc}=42.3, D_{sc}=9.73, P_{tot}=1.25, K_{ved}= 4.58, D_{ved}=0.325, P_{ved}=0.348).

starting the skin permeation experiment. As in the silicone membrane, the increase in partition coefficient, K, of parabens increased the skin concentration. The increment, however, was marked in the silicone membrane concentration, not in rat skin, except MP. This is due to the similar solubility parameter of parabens to that in the silicone membrane.

Fig. 8 shows the relation between the theoretical and observed skin concentrations of parabens. Although no 1:1 relationship was observed, a linear relation was found. When skin permeation data of a series of compounds are obtained,

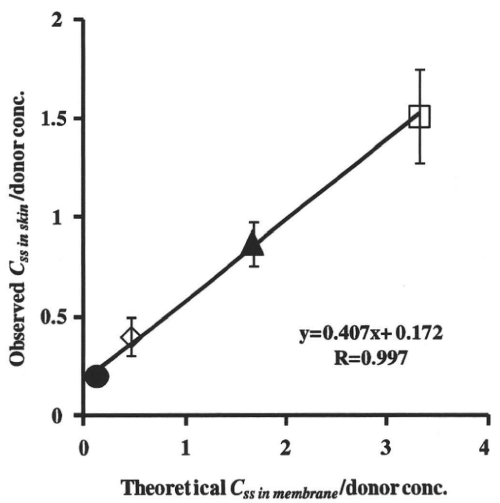

Fig. 12. Relationship between theoretical C_{ss} in silicone membrane/donor concentration and observed C_{ss} in rat skin/donor concentration. Symbols: see Fig. 3. Each data point represents the mean ± S.D. (n=3–8).

the skin concentration of the compounds may be theoretically calculated. The figure also contains the obtained permeation parameters of parabens in the figure legend, under the assumption that the skin membrane is one homogenous layer. Compared to the silicone membrane, lower P and D and higher K were observed in the rat skin. Unfortunately, the theoretical skin concentration of parabens was much higher than the observed skin concentration. This lack of a 1:1 relationship is due to the assumption that the skin is one homogenous layer.

Fig. 9 illustrates the relationship between K and silicone membrane and rat skin (11). The two K values have a linear relation. These results suggest that the skin concentration of parabens cannot be easily predicted by calculating the skin permeation profiles because of the simple assumption about the skin membrane.

Simulation of Skin Concentration of Parabens

We then assumed that skin consists of two diffusion layers, of which the first layer is the stratum corneum and the second layer is the viable epidermis and dermis. The partition coefficient from the vehicle to the stratum corneum and that to the viable epidermis and dermis was obtained from permeation data through full-thickness and stripped skin.

First, the stripped-skin permeability of parabens was measured. Fig. 10a and b show raw and normalized permeation profiles through stripped skin. Tape stripping of the stratum corneum increased the skin permeation of parabens, especially hydrophilic parabens such as MP.

Fig. 11 shows the relation between the observed and calculated skin concentrations. The figure also summarizes the obtained permeation parameters of parabens in the legend. The theoretical values are close to the observed values, although little difference was found, which may be dependent on the process of washing the skin surface. The two-layered model predicts the skin concentration of parabens from skin permeation experiments much better than the one-layered model of hairless rat skin. Human and animal skins have appendages, such as hair follicles and sweat ducts, as additional permeation pathways to the primary permeation pathway, the stratum corneum (21). The hydrophilic pathway and the lipophillic pathway play a role in the overall skin permeation of several compounds. The contribution of appendages and the hydrophilic pathway must be taken into account to better predict the skin concentration of materials from skin permeation profiles.

Fig. 12 shows the relationship between the theoretical concentration of parabens in the silicone membrane and the normalized observed concentration of parabens in hairless rat skin. The very high correlation coefficient, 0.997, between them suggests the high predictability of the skin concentration of parabens using silicone membrane permeation experiments.

We supposed a homogenous one-layered model for the silicone membrane and two-layered model consisted of stratum corneum and the following layer for the rat skin. Although these membrane models were different, their concentration-distance profiles and theoretical concentrations of drug or cosmetic ingredient in both the membranes can be expressed only by physical diffusion model. Thus, membrane concentration in the two-layered diffusion model can be easily replaced by that in the one-layered model using a mathematical approach. This is a reason why diffusion profile through silicone membrane is useful to predict the skin concentration of drugs or cosmetic ingredients.

In the near future, we plan to use broad compounds other than parabens, which are a simple series of compounds. We also plan to use several topical formulations, such as creams, ointments and patches. A silicone membrane permeation study using broad compounds from several formulations will produce a monogram of how to estimate the skin concentration of materials. All topical drugs have different target sites in skin tissues. Distribution of the skin concentration must be clarified from the shallow to deep layer in the near future. Since this is an alternative method to human and animal studies, it can be easily used by pharmaceutical and cosmetic companies to estimate the skin concentration after applying topical drug formulations and cosmetics.

CONCLUSION

The drug concentration in the silicone membrane and animal or human skin can be easily predicted using diffusion equations and membrane permeation data. This method can be applied to the design of cosmetic and topical pharmaceutical formulations. A silicone membrane can be used as an alternative membrane to human and animal skin.

ACKNOWLEDGEMENT

The authors are grateful to Mr. Yosuke Urabe and Mr. Masayasu Sugiura, Nagase & Co., Ltd. (Tokyo, Japan) for information on the silicone membrane.

REFERENCES

1. Knepp VM, Hadgraft J, Guy RH. Transdermal drug delivery: Problems and possibilities. Critical Rev Ther Drug Carrier Sys. 1987;4:13–37.
2. Singh P, Roberts MS. Iontophoretic transdermal delivery of salicylic acid and lidocaine to local subcutaneous structures. J Pharm Sci. 1993;82:127–31.
3. McNeill SC, Potts RO, Francoeur ML. Local enhanced topical delivery (LETD) of drugs: Does it truly exist? Pharm Res. 1992;9:1422–7.
4. Lodén M, Ungerth L, Serup J. Changes in European legislation make it timely to introduce a transparent market surveillance system for cosmetics. Acta Dermato-Venereol. 2007;87:485–92.
5. Toyoda H. Regulation of the animal experiments and testing in EU. Envir Mutagen Res. 2005;27:125–8.
6. Kolar R. Animal experimentation. Sci Eng Ethics. 2006;12:111–22.
7. Spielmann H. Animal use in the safety evaluation of chemicals: harmonization and emerging needs. ILAR J. 2002;43(Suppl):S11–7.
8. Leveque N, Raghavan SL, Lane ME, Hadgraft J. Use of a molecular form technique for the penetration of supersaturated solutions of salicylic acid across silicone membranes and human skin *in vitro*. Int J Pharm. 2006;318:49–54.
9. Ottaviani G, Martel S, Carrupt P. Parallel artificial membrane permeability assay: a new membrane for the fast prediction of passive human skin permeability. J Med Chem. 2006;49:3948–54.
10. Hatanaka T, Inuma M, Sugibayashi K, Morimoto Y. Prediction of skin permeability of drugs. I. Comparison with artificial membrane. Chem Pharm Bull. 1990;38:3452–9.
11. Geinoz S, Rey S, Boss G, Bunge AL, Guy RH, Carrupt PA, *et al.* Quantitative structure: permeation relationships for solute transport across silicone membranes. Pharm Res. 2002;19:1622–9.

12. Hasegawa T, Kim S, Tsuchida M, Isshiki Y, Kondo S, Sugibayashi K. Decrease in skin permeation and antibacterial effect of parabens by a polymeric additive, poly(2-methacryloyloxyethyl phosphorylcholine -cobutylmetacrylate). Chem Pharm Bull. 2005;53:271–6.
13. Herkenne C, Naik A, Kalia YN, Hadgraft J, Guy RH. Ibuprofen transport into and through skin from topical formulations: *In vitro-in vivo* comparison. J Invest Dermatol. 2007;127:135–42.
14. Hada N, Hasegawa T, Takahashi H, Ishibashi T, Sugibayashi K. Cultured skin loaded with tetracycline HCl and chloramphenicol as dermal delivery system: mathematical evaluation of the cultured skin containing antibiotics. J Control Release. 2005;108:341–50.
15. Scheuplein RJ, Blank IH. Mechanism of percutaneous absorption. IV. Penetration of nonelectrolytes (alcohols) from aqueous solutions and from pure liquids. J Invest Dermatol. 1973;60:286–96.
16. Scheuplein RJ. Mechanism of percutaneous absorption: transient diffusion and the relative importance of various routes of skin penetration. J Invest Dermatol. 1967;48:79–88.
17. Watanabe T, Hasegawa T, Takahashi H, Ishibashi T, Sugibayashi K. Utility of three-dimensional cultured human skin model as a tool to evaluate skin permeation drugs. Altern Animal Test Experiment. 2001;8:1–14.
18. Ghanem AH, Mahmoud H, Higuchi WI, Liu P. The effects of ethanol on the transport of lipophilic and polar permeants across hairless mouse skin: methods/validation of a novel approach. Int J Pharm. 1992;78:137–56.
19. Sugibayashi K, Hosoya K, Morimoto Y, Higuchi WI. Effect of the absorption enhancer, Azone, on the transport of 5-fluorouracil across hairless rat skin. J Pharm Pharmacol. 1985;37:578–80.
20. Pedersen S, Marra F, Nicoli S, Santi P. *In vitro* skin permeation and retention of parabens from cosmetic formulations. Int J Cosmetic Sci. 2007;29:361–7.
21. Moser K, Kriwet K, Naik A, Kalia YN, Guy RH. Passive skin penetration enhancement and its quantification *in vitro*. Eur J Pharm Biopharm. 2001;52:103–12.
22. Okumura M, Sugibayashi K, Ogawa K, Morimoto Y. Skin permeability of water-soluble drugs. Chem Pharm Bull. 1986; 37:1404–6.
23. Washitake M, Yajima T, Anmo T, Arita T, Hori R. Studies on percutaneous absorption of drugs. 3. Percutaneous absorption of drugs through damaged skin. Chem Pharm Bull. 1973;21:2444–51.
24. Sugibayashi K, Hayashi T, Morimoto Y. Simultaneous transport and metabolism of ethyl nicotinate in hairless rat skin after its topical application: the effect of enzyme distribution in skin. J Control Release. 1999;62:201–8.
25. Wilson BW, Walker CR. Regulation of newly synthesized acetylcholinesterase in muscle cultures treated with diisopropylfluorophosphate. Proc Natl Acad Sci USA. 1974;71:3194–8.
26. Sugibayashi K, Hayashi T, Matsumoto K, Hasegawa T. Utility of a three-dimensional cultured human skin model as a tool to ethyl nicotinate in skin. Drug Metabol Phamacokin. 2004;19: 352–62.
27. Nagaosa Y, Tanizaki M. Simultaneous determination of zinc(II) and iron(III) in human serum by liquid chromatography using post-column derivatization with 4-(2-pyridylazo)-resorcinol. J Liquid Chromat Related Technol. 1997;20:2357–66.
28. Kawase S, Kanno S, Ukai S. Determination of the herbicides paraquat and diquat in blood and urine by gas chromatography. J Chromat. 1984;283:231–40.
29. Izquierdo P, Gómez-Hens A, Pérez-Bendito D. Stopped-flow fluorometric determination of ampicillin in serum. Fresenius' J Analyt Chem. 1992;342:606–8.
30. Morimoto Y, Sugibayashi K, Hosoya K, Higuchi WI. Penetration enhancer effect of Azone on the transport of 5-fluorouracil across hairless rat skin. Int J Pharm. 1986;32:31–8.
31. Vaughan CD. Solubility effect in product, package, penetration and preservation. Cosmet Toilet. 1988;103:47–69.
32. Fedors RF. A method for estimating both the solubility parameters and molar volumes of liquids. Polym Eng Sci. 147 (1974).
33. LaPack MA, Tou JC, McGuffin VL, Enke CG. The correlation of membrane permselectivity with Hildebrand solubility parameters. J Membrane Sci. 1994;86:263–80.
34. Dias M, Hadgraft J, Lane ME. Influence of membrane-solvent-solute interactions on solute permeation in model membranes. Int J Pharm. 2007;336:108–14.

Life Sciences 87 (2010) 261–268

Contents lists available at ScienceDirect

Life Sciences

journal homepage: www.elsevier.com/locate/lifescie

Functional characterization of human and cynomolgus monkey UDP-glucuronosyltransferase 1A1 enzymes

Nobumitsu Hanioka [a,*], Natsuko Tanabe [a], Hideto Jinno [b], Toshiko Tanaka-Kagawa [b], Kenjiro Nagaoka [a], Shinsaku Naito [c], Akiko Koeda [d], Shizuo Narimatsu [a]

[a] Graduate School of Medicine, Dentistry and Pharmaceutical Sciences, Okayama University, 1-1-1 Tsushima-naka, Kita-ku, Okayama 700-8530, Japan
[b] Division of Environmental Chemistry, National Institute of Health Sciences, 1-18-1 Kamiyoga, Setagaya-ku, Tokyo 158-8501, Japan
[c] Research and Development Center, Otsuka Pharmaceutical Factory, Inc., 115 Kuguhara, Tateiwa, Muya-cho, Naruto, Tokushima 772-8601, Japan
[d] Department of Metabolism and Analytical Research, Ina Research Inc., 2148-188 Nishiminowa, Ina, Nagano 399-4501, Japan

ARTICLE INFO

Article history:
Received 17 March 2010
Accepted 30 June 2010

Keywords:
UDP-glucuronosyltransferase (UGT)
UGT1A1
7-Hydroxy-4-trifluoromethylcoumarin (7-HFC)
Estradiol at 3-hydroxy position (E-3OH)
7-Ethyl-10-hydroxycamptothecin (SN-38)
Human
Cynomolgus monkey

ABSTRACT

Aims: UDP-glucuronosyltransferase 1A1 (UGT1A1) plays important roles in the glucuronidation of various drugs and endogenous substances. Cynomolgus monkeys are regarded as experimental animals closer to humans in studies on safety evaluation and biotransformation for drug development. In this study, the similarities and differences in the enzymatic properties of UGT1A1 between humans and cynomolgus monkeys were precisely identified.

Main methods: Human and cynomolgus monkey UGT1A1s (humUGT1A1 and monUGT1A1, respectively) were cloned, and the corresponding proteins were heterologously expressed in insect cells. The enzymatic properties of UGT1A1 proteins were characterized by kinetic analysis of 7-hydroxy-4-trifluoromethylcoumarin (7-HFC), estradiol at 3-hydroxy position (E-3OH) and 7-ethyl-10-hydroxycamptothecin (SN-38) glucuronidation.

Key findings: There were no significant differences in the levels of kinetic parameters for 7-HFC, E-3OH and SN-38 glucuronidation between humans and cynomolgus monkeys in both enzyme sources of liver microsomes and recombinant UGT1A1s. 7-HFC and E-3OH glucuronidation by human liver microsomes exhibited biphasic and sigmoidal kinetics, respectively, whereas the kinetics by cynomolgus monkey liver microsomes fitted the typical Michaelis–Menten model. SN-38 glucuronidation by human and cynomolgus monkey liver microsomes exhibited autoactivation kinetics. In recombinant UGT1A1 enzymes expressed in insect cells, the kinetics of 7-HFC, E-3OH and SN-38 glucuronidation fitted the substrate inhibition (7-HFC glucuronidation) or Hill equation (E-3OH and SN-38 glucuronidation), and each glucuronidation showed the same kinetic profile between humans and cynomolgus monkeys.

Significance: These findings suggest that the enzymatic properties of human and cynomolgus monkey UGT1A1 enzymes are very similar.

Introduction

UDP-glucuronosyltransferases (UGTs) are membrane-bound enzymes that are localized inside the endoplasmic reticulum, and catalyze the conjugation of various endogenous substances (e.g. bile acids, bilirubin and steroids) and xenobiotics (e.g. drugs and environmental toxicants) to glucuronide (Ritter 2000; Tukey and Strassburg 2000). Consistent with their broad substrate profiles, UGTs are known to exist as a superfamily of independently regulated enzymes. The UGT superfamily is divided into many subfamilies on the basis of evolutionary divergence. Among the human UGT superfamily, two families (UGT1 and UGT2) and three subfamilies (UGT1A, UGT2A and UGT2B) are predominantly involved in glucuronidation (Mackenzie et al. 1997, 2005). The *UGT1A* gene is localized on chromosome 2q37 and encodes proteins with unique amino-terminal domains and identical carboxyl-terminal domains, which are formed from the alternate mRNA splicing of unique first exons with common exons 2–5. In contrast, *UGT2A* and *UGT2B* genes are clustered on chromosome 4q13 and individual UGT proteins are encoded by unique genes with six exons (Mackenzie et al. 1997, 2003, 2005; Guillemette 2003). Each UGT exhibits unique substrate and tissue specificities (Ritter 2000; Tukey and Strassburg 2000; Kiang et al. 2005).

UGT1A1 is expressed in the liver, bile duct, stomach and colon, and plays an important role in the detoxification of neurotoxic bilirubin by conjugating it with glucuronic acid for excretion in bile (Iyanagi et al. 1998; Tukey and Strassburg 2000). A reduced level of UGT1A1 activity has been reported to be associated with unconjugated hyperbilirubinemia (Crigler–Najjar syndrome and Gilbert's syndrome) (Mackenzie et al.

* Corresponding author. Tel./fax: +81 86 251 7943.
E-mail address: hanioka@pharm.okayama-u.ac.jp (N. Hanioka).

0024-3205/$ – see front matter © 2010 Elsevier Inc. All rights reserved.
doi:10.1016/j.lfs.2010.07.001

1997; Tukey and Strassburg 2000; Guillemette 2003). UGT1A1 also catalyzes the glucuronidation of 7-ethyl-10-hydroxycamptothecin (SN-38), the active metabolite of an anticancer drug, irinotecan (CPT-11, 7-ethyl-10-[4-(1-piperidino)-1-piperidino]carbonyloxy camptothecin), to form inactive SN-38 glucuronide (Iyer et al. 1998; Hanioka et al. 2001). Furthermore, wide interindividual variability in SN-38 glucuronide formation in hepatic tissues is known and has been shown to correlate with a *UGT1A1* genetic factor (Iyer et al. 1998, 1999; Guillemette 2003); therefore, *UGT1A1* polymorphisms have been regarded to be one of the most important factors for irinotecan efficacy and toxicity (Ando and Hasegawa 2005; Hasegawa et al. 2006; Ando et al. 2007).

Many UGT enzymes have been suggested to be expressed in hepatic and/or extrahepatic tissues of mammals, including humans, monkeys, rats and mice (Mackenzie et al. 1997, 2005; Tukey and Strassburg 2000), and the cDNAs of several isoforms have been cloned (http://som.flinders.edu.au/FUSA/ClinPharm/UGT/udgpa.html). In general, nonhuman primates, such as rhesus monkeys (*Macaca mulatta*) and cynomolgus monkeys (*Macaca fascicularis*), are regarded as experimental animals closer to humans in studies on safety evaluation and biotransformation for drug development; therefore, examination of the functional characterization of monkey UGT enzymes is an important aspect of drug metabolism research. Vallée et al. (2001) cloned cynomolgus monkey UGT1A1 (monUGT1A1) cDNA encoding an ortholog of human UGT1A1 (humUGT1A1), and qualitatively determined the catalytic activities toward estrogens of recombinant monUGT1A1 expressed in HEK293 cells; however, detailed kinetic analyses of xenobiotic glucuronidation by the recombinant enzyme were not included. Furthermore, there has been no report on the quantitative function characterization of human and cynomolgus monkey UGT1A1s using both enzyme sources of liver microsomes and recombinant enzymes.

The purpose of this study was to precisely identify the similarities and differences in the enzymatic properties of UGT1A1 between humans and cynomolgus monkeys. To achieve this, human and cynomolgus monkey UGT1A1 enzymes were heterologously expressed in insect cells, and the enzymatic properties were subsequently examined by kinetic analyses for the glucuronidation of 7-hydroxy-4-trifluoromethylcoumarin (7-HFC), estradiol at 3-hydroxy position (E-3OH), and SN-38.

Materials and methods

Materials

Three individual human liver microsomes (two men, 41 and 55 years old; one woman, 56 years old) and rabbit anti-human UGT1A1 antibody were purchased from BD Biosciences (San Jose, CA, USA). Three male cynomolgus monkey livers (4 years old, 2.7–2.9 kg) were supplied by Ina Research Inc. (Nagano, Japan). Cynomolgus monkey liver microsomes were prepared as described previously (Hanioka et al. 2006). The use of human and cynomolgus monkey livers for this study was approved by the ethics review boards of Okayama University. *Hin*dIII was purchased from Takara Bio (Shiga, Japan); pGEM-T vector was from Promega (Madison, WI, USA); pFastBac1 vector, Bac-to-Bac Baculovirus Expression System and *Spodoptera frugiperda* (Sf9) cells were from Invitrogen (Carlsbad, CA, USA); 7-HFC, 7-HFC glucuronide and E-3OH glucuronide were from Sigma-Aldrich (St. Louis, MO, USA); and estradiol was from Wako Pure Chemical Industries (Osaka, Japan). SN-38 and SN-38 glucuronide were supplied by Yakult Honsha (Tokyo, Japan). UDP-glucuronic acid was purchased from Nacalai Tesque (Kyoto, Japan); peroxidase-conjugated goat anti-rabbit immunoglobulin was from Zymed Laboratories (South San Francisco, CA, USA); and Enhanced Chemi-Luminescence Plus was from GE Healthcare Bio-Sciences (Little Chalfont, UK). All other chemicals and reagents used were of the highest quality commercially available.

Expression of recombinant UGT1A1 enzymes

humUGT1A1 cDNA was amplified by polymerase chain reaction (PCR) from humUGT1A1 cDNA cloned into pcDNA3.1 vector (Jinno et al. 2003) as a template using the forward primer 5′-AAGCTTAAAAAAATGGCTGTGGAGTCCCA-3′ and the reverse primer 5′-AAGCTTTCAATGGGTCTTGGATTTGTGGG-3′. The *Hin*dIII sites (underlined letters) were introduced at the 5′-end of the start codon and the 3′-end of the stop codon to facilitate subcloning into pFastBac1 vector. The cDNA encoding monUGT1A1 was amplified by nested PCR from cynomolgus monkey liver single-strand cDNA, prepared as described previously (Hanioka et al. 2006). The nucleotide sequences of the forward and reverse primers used were 5′-ATGGCTGTGGAGTCCCAAGGCAGACATC-3′ and 5′-CTCGAGTCTCAATGGGTCTTGGATTTGTGG-3′ for first PCR, and AAGCTTAAAAAAATGGCTGTGGAGTCCCA-3′ and 5′-AAGCTTTCAATGGGTCTTGGATTTGTGGG-3′ for second PCR. The PCR products of hum UGT1A1 and monUGT1A1 cDNAs were directly introduced into pGEM-T vector using TA cloning, and sequenced in both forward and reverse directions to confirm that there were no PCR errors. The cDNA fragments corresponding of humUGT1A1 and monUGT1A1 were cut from the pGEM-T plasmids with *Hin*dIII, and were subsequently subcloned into pFastBac1 vector digested with *Hin*dIII. The expression plasmids were sequenced to verify the correct orientation with respect to the promoter (polyhedrin promoter) for pFastBac1 vector.

Recombinant baculovirus carrying humUGT1A1 or monUGT1A1 cDNA was generated using the Bac-to-Bac Baculovirus Expression System according to the manufacturer's protocol. For protein expression, Sf9 cells (2.0×10^8 cells/flask) were infected with recombinant baculoviruses at a multiplicity of infection of 1.0. The cells were harvested at 72 h post-infection, and suspended in 50 mM Tris–HCl buffer (pH 7.4) containing 0.25 M sucrose, 0.1 mM dithiothreitol, 0.1 mM EDTA and 0.5 mM phenylmethylsulfonyl fluoride. The cell suspensions were sonicated 20 times with 10-s bursts, following by centrifugation at 105,000 *g* for 60 min to obtain membrane fractions. The resulting pellets were resuspended in 50 mM Tris–HCl (pH 7.4) containing 20% glycerol and stored at −80 °C until use. Total protein concentrations were determined by the method of Lowry et al. (1951) using bovine serum albumin as a standard.

Recombinant UGT1A1s (1.0 μg protein) as well as liver microsomes (20 μg protein) of humans and cynomolgus monkeys were separated by 10% sodium dodecyl sulfate-polyacrylamide gel electrophoresis (Laemmli 1970) and electrotransferred to a polyvinylidene fluoride sheet, as described by Towbin et al. (1979). The sheet was incubated with rabbit anti-human UGT1A1 antibody (diluted at 1:5000) as the primary antibody and then with peroxidase-conjugated goat anti-rabbit immunoglobulin (diluted at 1:5000) as the secondary antibody. Immunoreactive proteins were visualized with chemifluorescence (Enhanced ChemiLuminescence Plus), and band densities were relatively determined with ImageJ v1.42 (National Institute of Health Sciences, Bethesda, MD, USA).

Assay for UGT1A1-dependent enzymatic activities

Glucuronidation activities toward 7-HFC, E-3OH and SN-38 were determined by high-performance liquid chromatography as described previously with some modifications (Hanioka et al. 2001; Alkharfy and Frye 2002; Brill et al. 2006). The incubation mixture contained 7-HFC (1.0–200 μM), estradiol (0.5–100 μM) or SN-38 (0.5–100 μM) as a substrate, liver microsomes or recombinant UGT1A1s, 10 mM $MgCl_2$ and 5 mM UDP-glucuronic acid in a final volume of 500 μL of 50 mM Tris–HCl buffer (pH 7.4). The protein concentrations of liver microsomes and recombinant UGT1A1s were 10 and 50 μg/mL for 7-HFC and SN-38 glucuronidation assays, and 50 and 50 μg/mL for the E-3OH glucuronidation assay. The substrates were dissolved in

methanol/dimethyl sulfoxide (50:50, v/v) for 7-HFC and estradiol, and dimethyl sulfoxide/0.05 N NaOH (50:50, v/v) for SN-38. The final concentration of the organic solvent (methanol and/or dimethyl sulfoxide) in the incubation mixture was 1% (v/v). After preincubation for 2 min at 37 °C, the reaction was initiated by adding UDP-glucuronic acid. Incubation was performed for 10 min (7-HFC and SN-38 glucuronidation assay) or 20 min (E-3OH glucuronidation assay) at 37 °C and terminated by adding 50 μL of 10% phosphoric acid and vortexing. The samples were centrifuged at 12,000 *g* for 10 min at 4 °C. The supernatant was filtered with a polytetrafluoroethylene membrane filter (0.45 μm pore size; Millipore, Bedford, MA, USA), and a 20 μL portion of the filtrate was subjected to high-performance liquid chromatography.

The high-performance liquid chromatographic system consisted of an L-2130 pump (Hitachi, Tokyo, Japan), an L-2300 column oven (Hitachi), an L-2480 fluorescence detector (Hitachi), and a Rheodyne type 7725i (Hitachi) injector equipped with an Inertsil ODS-SP (4.6 mm i.d.×150 mm; GL Sciences, Tokyo, Japan) for 7-HFC and SN-38 glucuronidation assays or an Inertsil Ph (4.6 mm i.d.×150 mm; GL Sciences) for the E-3OH glucuronidation assay. The column was maintained at 40 °C. Data acquisition was accomplished using D-2000 Elite v1.1 software. 7-HFC glucuronide was eluted isocratically with 20 mM KH_2PO_4 (pH 3.5)/acetonitrile/methanol (62:26:12, v/v/v) at a flow rate of 1.0 mL/min. Fluorometric detection was performed with excitation at 328 nm and emission at 410 nm. Retention times of 7-HFC glucuronide and 7-HFC were 3.5 and 18.9 min, respectively. The limit of detection for 7-HFC glucuronide was 5.0 pmol/assay. E-3OH glucuronide was eluted isocratically with 20 mM KH_2PO_4 (pH 3.0)/acetonitrile (70:30, v/v) at a flow rate of 1.0 mL/min. Fluorometric detection was performed with excitation at 210 nm and emission at 300 nm. Retention times of E-3OH glucuronide and estradiol were 3.8 and 13.0 min, respectively. The limit of detection for E-3OH glucuronide was 10 pmol/assay. SN-38 glucuronide was eluted isocratically with 20 mM KH_2PO_4 containing 2 mM sodium 1-octanesulphonate (pH 2.5)/acetonitrile/methanol (72:22:6, v/v/v) at a flow rate of 1.0 mL/min. Fluorometric detection was performed with excitation at 370 nm and emission at 425 nm. Retention times of SN-38 glucuronide and SN-38 were 3.3 and 16.3 min, respectively. The limit of detection for SN-38 glucuronide was 0.2 pmol/assay. Standard curve samples spiked with 7-HFC glucuronide (10–5000 pmol/mL), E-3OH glucuronide (20–1000 pmol/mL) or SN-38 glucuronide (1.0–50 pmol/mL) for both assays were prepared in the same manner as incubation samples. Intra-day (n=5) and inter-day (n=5) precision did not exceed 10% in any of the assays.

Data analysis

Kinetic constants (K_m or S_{50}, V_{max}, and K_{si}) and the Hill coefficient (n) for 7-HFC, E-3OH and SN-38 glucuronidation were calculated by constructing velocity versus substrate concentration ([*S*]–[*V*]) and Eadie–Hofstee ([*V*/*S*]–[*V*]) plots using SigmaPlot v8.02 software (Systat Software, San Jose, CA, USA). The kinetic profile was estimated by comparison of r^2 among Michaelis–Menten, substrate inhibition, isoenzyme and Hill equations. In vitro clearance values were CL_{int} (V_{max}/K_m) or CL_{max} ($V_{max}/S_{50}{}^{*}(n-1)/(n(n-1)^{1/n})$. All values are expressed as the mean ± S.D. of three donors/animals or three separate experiments derived from independent preparations. Statistical comparisons were made with an unpaired two-tailed Student's *t*-test, and differences were considered significant when the p value was <0.05.

Results

Sequence analysis of humUGT1A1 and monUGT1A

Sequence analysis determined that humUGT1A1 and monUGT1A1 cDNA has an open reading frame of 1602 bp, encoding the respective proteins of 533 amino acids. The nucleotide sequence of humUGT1A1 was identical to that of cDNA characterized previously (GenBank accession no. NM_000463). In monUGT1A1, one silent mutation (1401A>G, Arg467Arg) was found compared with the cDNA cloned by Vallée et al. (2001) (GenBank accession no. AF104339). Fig. 1 shows the alignment of the deduced amino acid sequences between

```
humUGT1A1    1 MAVESQGGRPLVLGLLLCVLGPVVSHAGKILLIPVDGSHWLSMLGAIQQLQQRGHEIVVL 60
monUGT1A1    1 MAVESQGRHPLVLGLLLCVLGPVLCHAGKMLLIPVDGSHWLSMLGTIQQLQQRGHEIVVL 60
               *******  **************  **** *************** **************

humUGT1A1   61 APDASLYIRDGAFYTLKTYPVPFQREDVKESFVSLGHNVFENDSFLQRVIKTYKKIKKDS 120
monUGT1A1   61 APDASLYIREGAFYTLKTYPVPFQREDVKESFVSLGHNVFENDSFLRRVIKTYKKIKKDS 120
               ********* ************************************ **************

humUGT1A1  121 AMLLSGCSHLLHNKELMASLAESSFDVMLTDPFLPCSPIVAQYLSLPTVFFLHALPCSLE 180
monUGT1A1  121 AMLLSGCSHLLHNKELMASLAESSFDVMLTDPFLPCGPIVAQYLSLPTVFFLNALPCSLE 180
               ************************************ *************** *******

humUGT1A1  181 FEATQCPNPFSYVPRPLSSHSDHMTFLQRVKNMLIAFSQNFLCDVVYSPYATLASEFLQR 240
monUGT1A1  181 SEATQCPNPFSYVPRPLSAHSDHMTFLQRVKNMLIAFSQNFLCDVVYSPYATLASEFLQR 240
                ****************** ******************************************

humUGT1A1  241 EVTVQDLLSSASVWLFRSDFVKDYPRPIMPNMVFVGGINCLHQNPLSQEFEAYINASGEH 300
monUGT1A1  241 EVTVQNLLSSASVWLLRSDFVKDYPRPIMPNMAFIGGINCLHQSPLSQEFEAYINASGEH 300
               ***** ********* **************** * ******** *****************

humUGT1A1  301 GIVVFSLGSMVSEIPEKKAMAIADALGKIPQTVLWRYTGTRPSNLANNTILVKWLPQNDL 360
monUGT1A1  301 GIVVFSLGSMVAEIPEKKAMAIADALGKIPQTVLWRYTGTPPSNLANNTILVKWLPQNDL 360
               *********** ***************************** ********************

humUGT1A1  361 LGHPMTRAFITHAGSHGVYESICNGVPMVMMPLFGDQMDNAKRMETKGAGVTLNVLEMTS 420
monUGT1A1  361 LGHPMTRAFITHAGSHGIYEGICNGVPMVMMPLFGDQMDNAKRMETKGAGVTLNVLEMTS 420
               ***************** ** ****************************************

humUGT1A1  421 EDLENALKAVINDKSYKENIMRLSSLHKDRPVEPLDLAVFWVEFVMRHKGAPHLRPAAHD 480
monUGT1A1  421 EDLENALKAVINDKSYKENIMHLSSLHKDRPVEPLDLAVFWVEFVMRHKGAPHLRPAAHD 480
               ******************** ****************************************

humUGT1A1  481 LTWYQYHSLDVIGFLLAVVLTVAFITFKCCAYGYRKCLGKKGRVKKAHKSKTH 533
monUGT1A1  481 LTWYQYHSLDVIGFLLAIVLTVAFIAFKCCAYGYRKCFGKKGRVKKAHKSKTH 533
               ***************** ******* *********** ***************
```

Fig. 1. Deduced amino acid sequence alignment of humUGT1A1 and monUGT1A1. Asterisks indicate the same amino acid residues between humUGT1A1 and monUGT1A1.

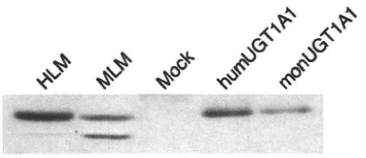

Fig. 2. Immunoblotting of liver microsomes and insect cell membranes expressing UGT1A1s of humans and cynomolgus monkeys. Representative results of pooled samples from three independent preparations are expressed. Protein levels applied were 1.0 μg/lane for recombinant UGT1A1s and 20 μg/lane liver microsomes. HLM, human liver microsomes; MLM, cynomolgus monkey liver microsomes.

humUGT1A1 and monUGT1A1. The homology between humUGT1A1 and monUGT1A1 was 95% at the amino acid level.

Expression of humUGT1A1 and monUGT1A1 enzymes

Human and cynomolgus monkey UGT1A1 enzymes were expressed separately in insect cells. Fig. 2 shows immunoblotting for liver microsomes and insect cell membranes expressing UGT1A1s of humans and cynomolgus monkeys using anti-human UGT1A1 antibody. All enzyme sources except the negative control (mock) yielded immunodetectable UGT1A1 protein; however, the staining band intensities of cynomolgus monkey liver microsomes and insect cells expressing monUGT1A1 were weak compared with those from enzyme sources in humans. The relative levels were human liver microsomes (100) and cynomolgus monkey liver microsomes (51), and humUGT1A1 (100) and monUGT1A1 (42), where human values were normalized to 100.

Enzymatic properties of humUGT1A1 and monUGT1A1 enzymes

Kinetic analyses of 7-HFC, E-3OH and SN-38 glucuronidation by recombinant humUGT1A1 and monUGT1A1 as well as by human and cynomolgus monkey liver microsomes were then performed. No activity in insect cell membranes of the negative control (mock) was detected with any substrate (data not shown). The plots ([*S*]–[*V*] and [*V*/*S*]–[*V*] plots) and parameters of kinetics are shown in Fig. 3 and Table 1 for 7-HFC glucuronidation, Fig. 4 and Table 2 for E-3OH glucuronidation, and Fig. 5 and Table 3 for SN-38 glucuronidation.

Table 1
Kinetic parameters for 7-HFC glucuronidation by liver microsomes and recombinant UGT1A1s of humans and cynomolgus monkeys.

	K_m (μM)	V_{max} (nmol/min/mg protein)	CL_{int} (μL/min/mg protein)	K_{si} (μM)
HLM				
High-affinity phase	2.58 ± 1.66	2.94 ± 1.43	1240 ± 250	
Low-affinity phase	30.1 ± 3.9	14.4 ± 6.8	479 ± 208	
MLM	16.1 ± 1.9	25.9 ± 2.9	1610 ± 100	
humUGT1A1	198 ± 47	7.10 ± 2.07	35.2 ± 2.9	99.6 ± 19.9
monUGT1A1	151 ± 74	3.90 ± 2.31	24.8 ± 3.0	161 ± 76

Each value represents the mean ± SD of three separate experiments derived from independent preparations. HLM, human liver microsomes; MLM, cynomolgus monkey liver microsomes.

7-HFC glucuronidation by human liver microsomes exhibited a biphasic kinetic profile, and K_m values for high- and low-affinity phases were 2.6 and 30 μM, respectively. V_{max} and CL_{int} values were 2.9 nmol/min/mg protein and 1200 μL/min/mg protein for the high-affinity phase, and 14 nmol/min/mg protein and 480 μL/min/mg protein for the low-affinity phase, respectively. In cynomolgus monkey liver microsomes, the kinetics of 7-HFC glucuronidation was monophasic with a K_m value of 16 μM. V_{max} and CL_{int} values were 1.8- and 1.3-fold higher than those of low- and high-affinity phases in human liver microsomes, respectively. 7-HFC glucuronidation by recombinant human and cynomolgus monkey UGT1A1s exhibited substrate inhibition kinetics with K_{si} values of 100 μM for humUGT1A1 and 160 μM for monUGT1A1. K_m, V_{max} and CL_{int} values

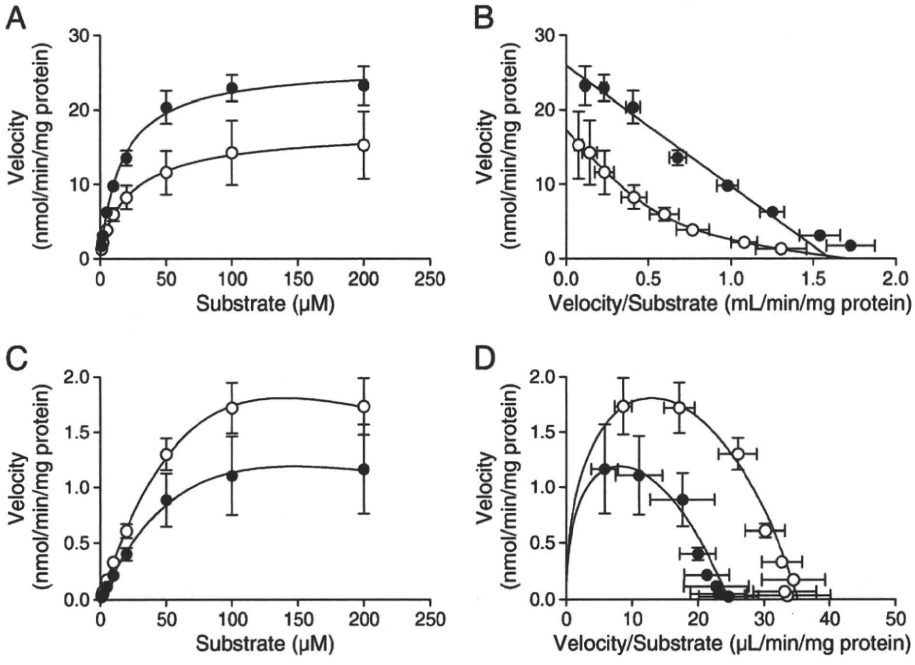

Fig. 3. Kinetics for 7-HFC glucuronidation by liver microsomes and insect cell membranes expressing UGT1A1s of humans and cynomolgus monkeys. Substrate concentrations were 1.0–200 μM. Each point represents the mean ± SD of three separate experiments derived from independent preparations. (A) [*S*]–[*V*] plots for liver microsomes; (B) [*V*/*S*]–[*V*] plots for liver microsomes; (C) [*S*]–[*V*] plots for insect cell membranes expressing UGT1A1s; (D) [*V*/*S*]–[*V*] plots for insect cell membranes expressing UGT1A1s. ○, human liver microsomes or humUGT1A1; ●, cynomolgus monkey liver microsomes or monUGT1A1.

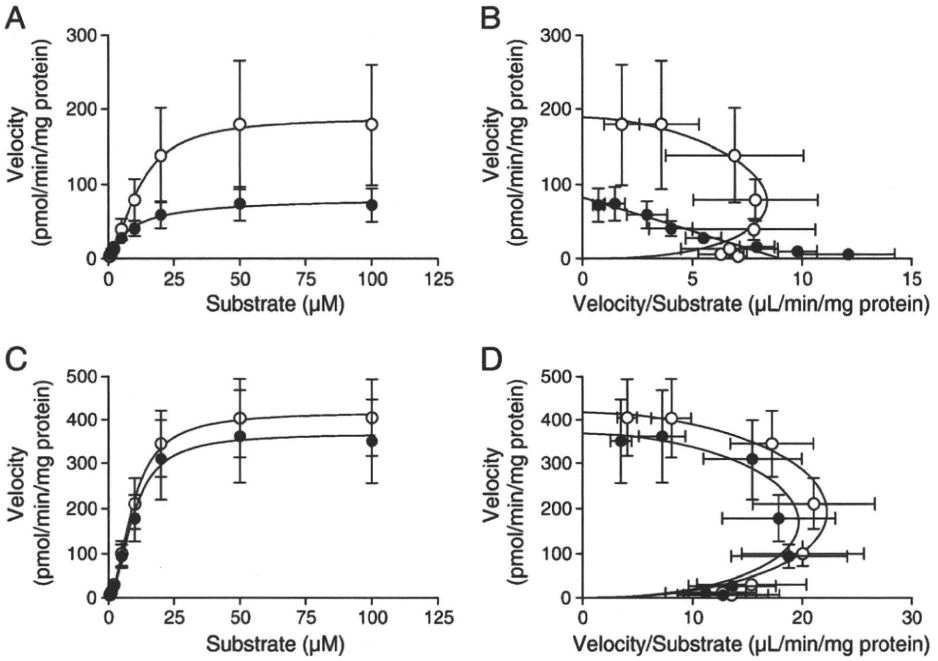

Fig. 4. Kinetics for E-3OH glucuronidation by liver microsomes and insect cell membranes expressing UGT1A1s of humans and cynomolgus monkeys. Substrate concentrations were 0.5–100 μM. Each point represents the mean ± SD of three separate experiments derived from independent preparations. (A) [*S*]–[*V*] plots for liver microsomes; (B) [*V*/*S*]–[*V*] plots for liver microsomes; (C) [*S*]–[*V*] plots for insect cell membranes expressing UGT1A1s; (D) [*V*/*S*]–[*V*] plots for insect cell membranes expressing UGT1A1s. ○, human liver microsomes or humUGT1A1; ●, cynomolgus monkey liver microsomes or monUGT1A1.

of humUGT1A1 were 200 μM, 7.1 nmol/min/mg protein and 35 μL/min/mg protein, respectively. The levels of monUGT1A1 were not significantly different from those of humUGT1A1.

E-3OH glucuronidation by human liver microsomes followed sigmoidal kinetics with n of 1.7, which manifests as a curvilinear [*V*/*S*]–[*V*] plot. S_{50}, V_{max} and CL_{max} values were 11 μM, 190 pmol/min/mg protein and 11 μL/min/mg protein, respectively. In contrast, the kinetics of E-3OH glucuronidation by cynomolgus monkey liver microsomes was fitted to the monophasic Michaelis–Menten model. K_m and CL_{int} values were comparable to those of S_{50} and CL_{max} for human liver microsomes, respectively, whereas the V_{max} value was 44% that of human liver microsomes. E-3OH by recombinant human and cynomolgus monkey UGT1A1s exhibited sigmoidal kinetics with n of 1.9 for both humUGT1A1 and monUGT1A1. S_{50}, V_{max} and CL_{max} values of humUGT1A1 were 9.5 μM, 420 pmol/min/mg protein and 30 μL/min/mg protein, respectively. The levels of monUGT1A1 were comparable to those of humUGT1A1.

SN-38 glucuronidation by liver microsomes and recombinant UGT1A1s of humans and cynomolgus monkeys exhibited sigmoidal kinetics. The n of liver microsomes and recombinant UGT1A1 of humans were 1.4 and 1.9, respectively. S_{50}, V_{max} and CL_{max} of humans were 7.4 μM, 49 pmol/min/mg protein and 4.2 μL/min/mg protein for liver microsomes, and 6.8 μM, 130 pmol/min/mg protein and 13 μL/min/mg protein for recombinant UGT1A1, respectively. These parameter levels for sigmoidal kinetics of cynomolgus monkeys were comparable to those of humans in both liver microsomes and recombinant UGT1A1.

Table 2
Kinetic parameters for E-3OH glucuronidation by liver microsomes and recombinant UGT1A1s of humans and cynomolgus monkeys.

	K_m or S_{50} (μM)	V_{max} (pmol/min/mg protein)	n	CL_{int} or CL_{max} (μL/min/mg protein)
HLM	11.3 ± 0.7	189 ± 86	1.66 ± 0.15	10.5 ± 4.7
MLM	8.79 ± 2.04	82.4 ± 28.9		9.23 ± 1.07
humUGT1A1	9.47 ± 0.39	418 ± 93	1.86 ± 0.06	29.6 ± 7.0
monUGT1A1	9.42 ± 0.15	368 ± 103	1.85 ± 0.05	26.2 ± 8.0

Each value represents the mean ± SD of three separate experiments derived from independent preparations. HLM, human liver microsomes; MLM, cynomolgus monkey liver microsomes.

Discussion

UGT1A1, a member of the UGT superfamily, plays an important role in the glucuronidation of various endogenous substances and medicines (Ritter 2000; Tukey and Strassburg 2000; Kiang et al. 2005). UGT1A1 activity and expression have also been shown to be influenced by genetic, physiological and environmental factors (Tukey and Strassburg 2000; Mackenzie et al. 2003). Although monkeys, including cynomolgus monkeys, are commonly used as an animal model for the development of medicines, and particularly for the characterization of pharmacokinetics and toxicological properties of novel molecules, little is known about the enzymatic properties of monkey UGT enzymes. The functional evaluation of human and cynomolgus monkey UGT1A1 enzymes should provide important information for the prediction and extrapolation of drug metabolism. Enzymatic activities in insect cells expressing human and cynomolgus monkey UGT1A1s were therefore investigated by kinetic analysis. To this end, we used 7-HFC, E-3OH and SN-38 glucuronidation as the probes for UGT1A1.

The expression of UGT1A1 proteins was confirmed by Western blot analysis. Anti-human UGT1A1 antibody recognized the corresponding UGT1A1s in livers microsomes and insect cell membranes expressing UGT1A1s of humans and cynomolgus monkeys, and the intensities of staining bands for liver microsomes and recombinant UGT1A1 of cynomolgus monkeys were about 50–40% those of humans. This phenomenon is thought to occur because the cross-reactivity with UGT1A1 proteins of the antibody used in this study differed between human and cynomolgus monkey UGT1A1s.

The active site of UGT enzymes is on the luminal side of the endoplasmic reticulum, resulting in an in vitro latency (Radominska-Pandya et al. 1999; Tukey and Strassburg 2000). To overcome this phenomenon in vitro, alamethicin (pore-forming agent) is commonly used as an alternative to detergents (Fisher et al. 2000a, 2001).

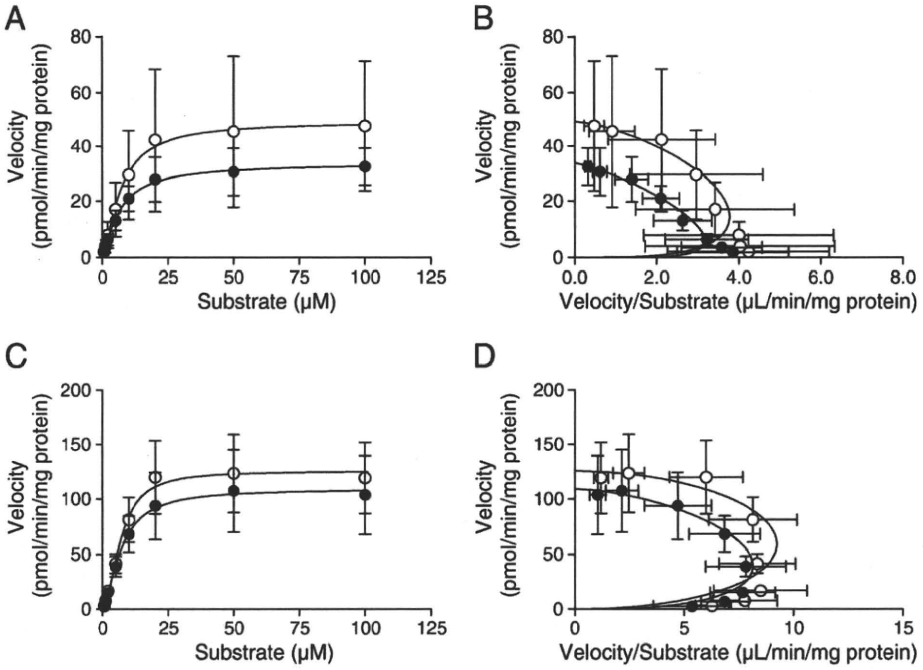

Fig. 5. Kinetics for SN-38 glucuronidation by liver microsomes and insect cell membranes expressing UGT1A1s of humans and cynomolgus monkeys. Substrate concentrations were 0.5–100 μM. Each point represents the mean ± SD of three separate experiments derived from independent preparations. (A) [*S*]–[*V*] plots for liver microsomes; (B) [*V*/*S*]–[*V*] plots for liver microsomes; (C) [*S*]–[*V*] plots for insect cell membranes expressing UGT1A1s; (D) [*V*/*S*]–[*V*] plots for insect cell membranes expressing UGT1A1s. ○, human liver microsomes or humUGT1A1; ●, cynomolgus monkey liver microsomes or monUGT1A1.

Although we do not have evidence of the effect of alamethicin on the kinetic profile of glucuronidation, the optimum concentration of 7-HFC glucuronidation for human liver microsomes differed among substrate concentrations in our preliminary study. Therefore, to evaluate uniformly the results of kinetic analysis, the glucuronidation activities toward 7-HFC, estradiol and SN-38 in human liver microsomes and recombinant UGT1A without alamethicin were determined in this study.

7-HFC glucuronidation in humans has been reported to be catalyzed by several UGT1A and UGT2B isoforms, except UGT1A4, although there is no information on the kinetics (Ghosal et al. 2004; Kaku et al. 2004). These reports showed that UGT1A6 and UGT1A9 have higher activities among UGT isoforms expressed in the liver, and the activity of UGT1A1 is 12–32% that of UGT1A6 and UGT1A9. In this study, the kinetics of 7-HFC glucuronidation by human liver microsomes was biphasic, and the K_m value of recombinant humUGT1A1 was remarkably low compared with those of high- and low-affinity phases, supporting the observation of the 7-HFC activity of each UGT isoform in previous reports (Ghosal et al. 2004; Kaku et al. 2004). In contrast, the kinetics of 7-HFC glucuronidation by cynomolgus monkey liver microsomes was monophasic, followed by the Michaelis–Menten model, and the expression profile of UGT isoforms in the liver was considered to be extensively different between humans and cynomolgus monkeys. In recombinant UGT1A1s, the glucuronidation of 7-HFC showed substrate inhibition kinetics in both humans and cynomolgus monkeys, and there was no significant difference in the levels of kinetic constants between humUGT1A1 and monUGT1A1. The kinetic profile of 7-HFC glucuronidation by liver microsomes and recombinant UGT1A1s of humans and cynomolgus monkeys was first suggested in this study.

Table 3
Kinetic parameters for SN-38 glucuronidation by liver microsomes and recombinant UGT1A1s of humans and cynomolgus monkeys.

	S_{50} (μM)	V_{max} (pmol/min/mg protein)	n	CL_{int} (μL/m i n/mg protein)
HLM	7.44 ± 0.83	49.4 ± 26.5	1.35 ± 0.14	4.21 ± 2.49
MLM	6.74 ± 0.38	33.8 ± 8.0	1.21 ± 0.04	3.29 ± 0.86
humUGT1A1	6.75 ± 0.50	126 ± 35	1.89 ± 0.08	12.5 ± 3.1
monUGT1A1	7.00 ± 1.59	110 ± 39	1.61 ± 0.28	9.87 ± 1.79

Each value represents the mean ± SD of three separate experiments derived from independent preparations. HLM, human liver microsomes; MLM, cynomolgus monkey liver microsomes.

Glucuronidation of E-3OH is a useful probe for UGT1A1 activity in humans (Senafi et al. 1994; Ritter 2000; Court 2005). The kinetics of E-3OH glucuronidation by human liver microsomes and recombinant UGT1A1s (humUGT1A1 and monUGT1A1) best fitted the Hill equation, indicating substrate activation, and agreed with the previous report of Fisher et al. (2000b); however, the kinetics of cynomolgus monkey liver microsomes appeared to follow a typical Michaelis–Menten model. Fisher et al. (2000b) have also suggested that E-3OH glucuronidation by human liver microsomes exhibited atypical kinetics. Although the cause of the species difference in the kinetics of E-3OH glucuronidation by liver microsomes is unclear at present, it may be due to the turnover level in each sample, as suggested for interindividual differences of E-3OH activities in human liver microsomes (Fischer et al. 2000b). K_m or S_{50} values of recombinant humUGT1A1 and monUGT1A1 were comparable to those of human and cynomolgus monkey liver microsomes, respectively, and no significant species difference in the kinetic parameter levels was observed. Thus, it was suggested that UGT1A1 is the predominant isoform responsible for E-3OH glucuronidation in both species.

We further determined SN-38 glucuronidation activity in liver microsomes and recombinant UGT1A1s of humans and cynomolgus monkeys. SN-38 is reportedly catalyzed mainly by UGT1A1 in humans (Hanioka et al. 2001; Gagné et al. 2002; Court 2005; Kiang et al. 2005). The kinetics of SN-38 glucuronidation as well as E-3OH glucuronidation was sigmoidal in all enzyme sources, and there were no significant differences in the kinetic levels of SN-38 glucuronidation by liver microsomes and recombinant UGT1A1s between humans and cynomolgus monkeys. The K_m values of human liver microsomes and

recombinant human UGT1A1 expressing insect or COS-1 cells have been reported to be 3.7–36 and 7.5–24 μM, respectively (Hanioka et al. 2001; Gagné et al. 2002; Jinno et al. 2003; Zhang et al. 2007). The S_{50} values of human liver microsomes (7.4 μM) and insect cell membranes expressing humUGT1A1 (6.8 μM) obtained in this study were comparable to those of K_m values in other studies. Thus, there were no remarkable species differences in the kinetics of 7-HFC, E-3OH and SN-38 glucuronidation by liver microsomes and recombinant UGT1A1 between humans and cynomolgus monkeys. The kinetic profile for glucuronidation was extensively different according to substrates and enzyme sources, although the reason for this phenomenon is unclear at present.

Comparison of the primary amino acid sequence of cynomolgus monkey UGT1A enzymes with the corresponding human enzymes revealed more than 90% identity. In addition, comparison of the conserved carboxyl-region demonstrates 97% sequence identity between humans and cynomolgus monkeys (Barbier and Bélanger 2003). These data generally illustrate the elevated homology of UGT1A isoforms and suggest similar *UGT1A* gene organization between humans and cynomolgus monkeys. Based on this information, Barbier and Bélanger (2003) have found that enzymatic activities toward estrogen (estradiol, estriol and estron) of UGT1As (UGT1A1 and UGT1A9) are similar between humans and cynomolgus monkeys, and reviewed the relevance of cynomolgus monkeys as an animal model for the study of steroid glucuronidation. The glucuronidation abilities toward 7-HFC and SN-38 as well as estradiol of monUGT1A1 were suggested to be also very similar to those of humUGT1A1 in this study; however, with respect to UGT1A6, we have demonstrated that the enzymatic properties of UGT1A6 were extensively different between humans and cynomolgus monkeys using serotonin and 4-methylumbelliferone glucuronidation as probes (Hanioka et al. 2006). The similarities and differences in the enzymatic properties of UGT1As between humans and cynomolgus monkeys seem to be isoform dependent.

In conclusion, we expressed human and cynomolgus monkey UGT1A1 enzymes in insect cells, and showed 7-HFC, E-3OH and SN-38 glucuronidation in recombinant UGT1A1s as well as in liver microsomes of humans and cynomolgus monkeys. The kinetics of 7-HFC and E-3OH glucuronidation by human liver microsomes were biphasic and sigmoidal, respectively, whereas the kinetics by cynomolgus monkey liver microsomes was monophasic followed by the Michaelis–Menten model. SN-38 glucuronidation by human and cynomolgus monkey liver microsomes exhibited autoactivation kinetics. The kinetics of 7-HFC, E-3OH and SN-38 glucuronidation by recombinant humUGT1A1 and monUGT1A1 fitted substrate inhibition (7-HFC glucuronidation) or the Hill equation (E-3OH and SN-38 glucuronidation), and each glucuronidation showed the same kinetic profile between humans and cynomolgus monkeys. There were no significant differences in the levels of kinetic parameters for 7-HFC, E-3OH and SN-38 glucuronidation between humans and cynomolgus monkeys in both liver microsomes and recombinant UGT1A1s. These findings suggest that human and cynomolgus monkey UGT1A1 enzymes have high homology in their amino acid sequences, and that their enzymatic properties are very similar. The information gained in this study should help with the in vitro–in vivo extrapolation of drug metabolism.

Conflict of interest statement

The authors have no duality of interest to declare.

Acknowledgments

This work was supported in part by a Grant-in-Aid for Scientific Research (20590121) from the Ministry of Education, Culture, Sports, Science and Technology of Japan; and in part by a Health and Labor Sciences Research Grant (21340701) from the Ministry of Health, Labor and Welfare of Japan.

References

Alkharfy KM, Frye RF. Sensitive liquid chromatographic method using fluorescence detection for the determination of estradiol 3- and 17-glucuronides in rat and human liver microsomal incubations: formation kinetics. Journal of Chromatography B: Analytical Technologies in the Biomedical and Life Sciences 774 (1), 33–38, 2002.

Ando Y, Hasegawa Y. Clinical pharmacogenetics of irinotecan (CPT-11). Drug Metabolism Reviews 37 (3), 565–574, 2005.

Ando Y, Fujita K, Sasaki Y, Hasegawa Y. *UGT1A1*6* and *UGT1A1*27* for individualized irinotecan chemotherapy. Current Opinion in Molecular Therapeutics 9 (3), 258–262, 2007.

Barbier O, Bélanger A. The cynomolgus monkey (*Macaca fascicularis*) is the best animal model for the study of steroid glucuronidation. The Journal of Steroid Biochemistry and Molecular Biology 85 (2–5), 235–245, 2003.

Brill SS, Furimsky AM, Ho MN, Furniss MJ, Li Y, Green AG, Bradford WW, Green CE, Kapetanovic IM, Iyer LV. Glucuronidation of trans-resveratrol by human liver and intestinal microsomes and UGT isoforms. The Journal of Pharmacy and Pharmacology 58 (4), 469–479, 2006.

Court MH. Isoform-selective probe substrates for in vitro studies of human UDP-glucuronosyltransferases. Methods in Enzymology 400, 104–116, 2005.

Fisher MB, Campanale K, Ackermann BL, VandenBranden M, Wrighton SA. In vitro glucuronidation using human liver microsomes and the pore-forming peptide alamethicin. Drug Metabolism and Disposition 28 (5), 560–566, 2000a.

Fisher MB, Vandenbranden M, Findlay K, Burchell B, Thummel KE, Hall SD, Wrighton SA. Tissue distribution and interindividual variation in human UDP-glucuronosyltransferase activity: relationship between UGT1A1 promoter genotype and variability in a liver bank. Pharmacogenetics 10 (8), 727–739, 2000b.

Fisher MB, Paine MF, Strelevitz TJ, Wrighton SA. The role of hepatic and extrahepatic UDP-glucuronosyltransferases in human drug metabolism. Drug Metabolism Reviews 33 (3–4), 273–297, 2001.

Gagné JF, Montminy V, Belanger P, Journault K, Gaucher G, Guillemette C. Common human *UGT1A* polymorphisms and the altered metabolism of irinotecan active metabolite 7-ethyl-10-hydroxycamptothecin (SN-38). Molecular Pharmacology 62 (3), 608–617, 2002.

Ghosal A, Hapangama N, Yuan Y, Achanfuo-Yeboah J, Iannucci R, Chowdhury S, Alton K, Patrick JE, Zbaida S. Identification of human UDP-glucuronosyltransferase enzyme (s) responsible for the glucuronidation of posaconazole (Noxafil). Drug Metabolism and Disposition 32 (2), 267–271, 2004.

Guillemette C. Pharmacogenomics of human UDP-glucuronosyltransferase enzymes. The Pharmacogenomics Journal 3 (3), 136–158, 2003.

Hanioka N, Ozawa S, Jinno H, Ando M, Saito Y, Sawada J. Human liver UDP-glucuronosyltransferase isoforms involved in the glucuronidation of 7-ethyl-10-hydroxycamptothecin. Xenobiotica 31 (10), 687–699, 2001.

Hanioka N, Takeda Y, Jinno H, Tanaka-Kagawa T, Naito S, Koeda A, Shimizu T, Nomura M, Narimatsu S. Functional characterization of human and cynomolgus monkey UDP-glucuronosyltransferase 1A6 enzymes. Chemico-Biological Interactions 164 (1–2), 136–145, 2006.

Hasegawa Y, Ando Y, Ando M, Hashimoto N, Imaizumi K, Shimokata K. Pharmacogenetic approach for cancer treatment-tailored medicine in practice. Annals of the New York Academy of Sciences 1086, 223–232, 2006.

Iyanagi T, Emi Y, Ikushiro S. Biochemical and molecular aspects of genetic disorders of bilirubin metabolism. Biochimica et Biophysica Acta 1407 (3), 173–184, 1998.

Iyer L, King CD, Whitington PF, Green MD, Roy SK, Tephly TR, Coffman BL, Ratain MJ. Genetic predisposition to the metabolism of irinotecan (CPT-11). Role of uridine diphosphate glucuronosyltransferase isoform 1A1 in the glucuronidation of its active metabolite (SN-38) in human liver microsomes. The Journal of Clinical Investigation 101 (4), 847–854, 1998.

Iyer L, Hall D, Das S, Mortell MA, Ramírez J, Kim S, Di Rienzo A, Ratain MJ. Phenotype-genotype correlation of in vitro SN-38 (active metabolite of irinotecan) and bilirubin glucuronidation in human liver tissue with UGT1A1 promoter polymorphism. Clinical Pharmacology and Therapeutics 65 (5), 576–582, 1999.

Jinno H, Tanaka-Kagawa T, Hanioka N, Saeki M, Ishida S, Nishimura T, Ando M, Saito Y, Ozawa S, Sawada J. Glucuronidation of 7-ethyl-10-hydroxycamptothecin (SN-38), an active metabolite of irinotecan (CPT-11), by human UGT1A1 variants, G71R, P229Q, and Y486D. Drug Metabolism and Disposition 31 (1), 108–113, 2003.

Kaku T, Ogura K, Nishiyama T, Ohnuma T, Muro K, Hiratsuka A. Quaternary ammonium-linked glucuronidation of tamoxifen by human liver microsomes and UDP-glucuronosyltransferase 1A4. Biochemical Pharmacology 67 (11), 2093–2102, 2004.

Kiang TK, Ensom MH, Chang TK. UDP-glucuronosyltransferases and clinical drug-drug interactions. Pharmacology & Therapeutics 106 (1), 97–132, 2005.

Laemmli UK. Cleavage of structural proteins during the assembly of the head of bacteriophage T4. Nature 227 (5259), 680–685, 1970.

Lowry OH, Rosebrough NJ, Farr A, Randall RJ. Protein measurement with the Folin phenol reagent. The Journal of Biological Chemistry 193 (1), 265–275, 1951.

Mackenzie PI, Owens IS, Burchell B, Bock KW, Bairoch A, Bélanger A, Fournel-Gigleux S, Green M, Hum DW, Iyanagi T, Lancet D, Louisot P, Magdalou J, Chowdhury JR, Ritter JK, Schachter H, Tephly TR, Tipton KF, Nebert DW. The UDP glycosyltransferase gene superfamily: recommended nomenclature update based on evolutionary divergence. Pharmacogenetics 7 (4), 255–269, 1997.

Mackenzie PI, Gregory PA, Gardner-Stephen DA, Lewinsky RH, Jorgensen BR, Nishiyama T, Xie W, Radominska-Pandya A. Regulation of UDP glucuronosyltransferase genes. Current Drug Metabolism 4 (3), 249–257, 2003.

Mackenzie PI, Bock KW, Burchell B, Guillemette C, Ikushiro S, Iyanagi T, Miners JO, Owens IS, Nebert DW. Nomenclature update for the mammalian UDP glycosyltransferase (*UGT*) gene superfamily. Pharmacogenetics and Genomics 15 (10), 677–685, 2005.

Radominska-Pandya A, Czernik PJ, Little JM, Battaglia E, Mackenzie PI. Structural and functional studies of UDP-glucuronosyltransferases. Drug Metabolism Reviews 31 (4), 817–899, 1999.

Ritter JK. Roles of glucuronidation and UDP-glucuronosyltransferases in xenobiotic bioactivation reactions. Chemico-Biological Interactions 129 (1–2), 171–193, 2000.

Senafi SB, Clarke DJ, Burchell B. Investigation of the substrate specificity of a cloned expressed human bilirubin UDP-glucuronosyltransferase: UDP-sugar specificity and involvement in steroid and xenobiotic glucuronidation. The Biochemical Journal 303 (Pt 1), 233–240, 1994.

Towbin H, Staehelin T, Gordon J. Electrophoretic transfer of proteins from polyacrylamide gels to nitrocellulose sheets: procedure and some applications. Proceedings of the National Academy of Sciences of the United States of America 76 (9), 4350–4354, 1979.

Tukey RH, Strassburg CP. Human UDP-glucuronosyltransferases: metabolism, expression, and disease. Annual Review of Pharmacology and Toxicology 40, 581–616, 2000.

Vallée M, Albert C, Beaudry G, Hum DW, Bélanger A. Isolation and characterization of the monkey UDP-glucuronosyltransferase cDNA clone monUGT1A01 active on bilirubin and estrogens. The Journal of Steroid Biochemistry and Molecular Biology 77 (4–5), 239–249, 2001.

Zhang D, Zhang D, Cui D, Gambardella J, Ma L, Barros A, Wang L, Fu Y, Rahematpura S, Nielsen J, Donegan M, Zhang H, Humphreys WG. Characterization of the UDP glucuronosyltransferase activity of human liver microsomes genotyped for the *UGT1A1*28* polymorphism. Drug Metabolism and Disposition 35 (12), 2270–2280, 2007.

Arch Toxicol (2010) 84:363–371
DOI 10.1007/s00204-009-0504-1

TOXICOKINETICS AND METABOLISM

Functional characterization of human cytochrome P450 2E1 allelic variants: in vitro metabolism of benzene and toluene by recombinant enzymes expressed in yeast cells

Nobumitsu Hanioka · Maki Yamamoto · Toshiko Tanaka-Kagawa · Hideto Jinno · Shizuo Narimatsu

Received: 16 August 2009 / Accepted: 9 December 2009 / Published online: 24 December 2009

Abstract Benzene and toluene are common organic solvents currently in worldwide industrial usage, which are metabolized mainly by hepatic cytochrome P450 2E1 (CYP2E1) in humans. Genetic polymorphism of *CYP2E1* in 5′-flanking and coding regions has been found previously in Caucasian and Chinese populations. In this study, the effects of *CYP2E1* alleles causing amino acid substitutions (*CYP2E1*2*, *CYP2E1*3* and *CYP2E1*4*; wild-type, *CYP2E1.1A*) on benzene hydroxylation and toluene methylhydroxylation were studied using recombinant CYP2E1 enzymes of wild-type (CYP2E1.1) and variants (CYP2E1.2 having Arg76His, CYP2E1.3 having Val389Ile and CYP2E1.4 having Val179Ile) expressed in yeast cells. The K_m, V_{max} and CL_{int} values of CYP2E1.1 were 10.1 mM, 9.38 pmol/min/pmol CYP and 0.99 nL/min/pmol CYP for benzene hydroxylation, and 3.97 mM, 19.9 pmol/min/pmol CYP and 5.26 nL/min/pmol CYP for toluene methylhydroxylation, respectively. The K_m, V_{max} and CL_{int} values for benzene and toluene metabolism of CYP2E1.2, CYP2E1.3 and CYP2E1.4 were comparable to those of wild-type CYP2E1. These findings may mean that the polymorphic alleles of *CYP2E1* causing amino acid substitutions are not directly associated with the metabolic activation of benzene and toluene. The information gained in this study should help to identify the variations in the toxicity of environmental pollutants.

Keywords Benzene · Toluene · Metabolism · Cytochrome P450 2E1 (CYP2E1) · Genetic polymorphism

N. Hanioka (✉) · M. Yamamoto · S. Narimatsu
Graduate School of Medicine, Dentistry and Pharmaceutical Sciences, Okayama University, 1-1-1 Tsushima-naka, Kita-ku, Okayama 700-8530, Japan
e-mail: hanioka@pharm.okayama-u.ac.jp

T. Tanaka-Kagawa · H. Jinno
Division of Environmental Chemistry, National Institute of Health Sciences, 1-18-1 Kamiyoga, Setagaya-ku, Tokyo 158-8501, Japan

Introduction

Benzene and toluene are organic solvents widely used in a variety of industries and can also be encountered as household products or sniffing solvents. These compounds have been suggested to cause hematotoxicity, genotoxicity or carcinogenicity in humans (Fishbein 1988; Lauwerys and Buchet 1988; McMichael 1988; Snyder et al. 1993). It is considered that the urinary metabolites of benzene (glucuronide/sulfate conjugates of hydroxylated compounds (phenol, hydroquinone and catechol), *trans*, *trans*-muconic acid and *S*-phenylmercapturic acid) and toluene (hippuric acid and glucuronide/sulfate conjugates of *o*-cresol for toluene) are very important indices for the biological monitoring of individuals exposed to these compounds (Fishbein 1984, 1985).

Benzene has been shown to be metabolized to benzene oxide by hepatic cytochrome P450 (CYP) enzymes (mainly CYP2E1) in mammals (Koop et al. 1989; Guengerich et al. 1991; Nakajima et al. 1990, 1993). Benzene oxide is non-enzymatically rearranged to phenol, which can undergo another CYP oxidation to give hydroquinone (Kalf 1987; Koop et al. 1989; Snyder and Hedli 1996). The toxicity of benzene has been suggested to arise from free radicals formed when metabolites such as hydroquinone are further oxidized to form semiquinones (Greenlee et al. 1981; Smith et al. 1989; Snyder et al. 1993). Toluene metabolism in mammals has also been reported to catalyze CYP

enzymes to benzyl alcohol and *o*- and *p*-cresol (Nakajima et al. 1993; Hanioka et al. 1995; Tassaneeyakul et al. 1996; Kim et al. 1997). In rats and humans, the aliphatic hydroxylation forming benzyl alcohol as the major metabolic pathway is catalyzed by mainly CYP2E1, whereas the aromatic hydroxylation forming *o*- and *p*-cresol as the minor metabolic pathways is catalyzed by not only CYP2E1 but also by other CYP isoforms, such as CYP1A2 and CYP2Bs (Nakajima et al. 1991, 1992, 1993, 1997; Kim et al. 1997).

Members of the CYP superfamily catalyze the oxidative metabolism of exogenous compounds, such as drugs and environmental pollutants, as well as endogenous substances, such as steroids and fatty acids (Gonzalez 1990; Nelson et al. 1996; Rendic and Di Carlo 1997). CYP2E1 is expressed mainly in the liver and metabolizes compounds of relatively low molecular weight (Gonzalez 1990; Ingelman-Sundberg et al. 1993; Nelson et al. 1996). It has been suggested that there are large inter-individual variations in the protein level and catalytic activity of CYP2E1 in human liver microsomes (Yoo et al. 1988; Shimada et al. 1994). Previous in vivo studies of Caucasian populations using chlorzoxazone as a probe drug reported a several-fold variation in clearance with a normal distribution of activities and suggested that such variation was caused in part by the genetic polymorphism of *CYP2E1* (Kim and O'Shea 1995; Lucas et al. 1995).

Twelve allelic variants have been identified using restriction fragment polymorphism analysis or DNA sequencing to date (http://www.cypalleles.ki.se/cyp2e1.htm). In the coding region, three allelic variants termed *CYP2E1*2* (227G > A, Arg76His), *CYP2E1*3* (1165G > A, Val389Ile) and *CYP2E1*4* (535G > A, Val179Ile) with amino acid substitutions have been found in Caucasian and Chinese populations at frequencies of 1.3–2.6% (Hu et al. 1997; Fairbrother et al. 1998). One variant, *CYP2E1*2*, has been reported to affect the metabolic ability toward chlorzoxazone and 4-nitrophenol of the CYP2E1 enzyme (Hu et al. 1997; Fairbrother et al. 1998; Hanioka et al. 2003); however, there has been no report about the effect of genetic polymorphism of *CYP2E1* on the metabolism of environmental pollutions.

Since CYP2E1 metabolizes volatile organic compounds, such as benzene and toluene, the genetic polymorphism of *CYP2E1* has been regarded as an important environmental risk factor similar to those of *N*-acetyltransferase and glutathione *S*-transferase (Brockmöller et al. 1996; Thier et al. 2003). The purpose of this study was to clarify whether the amino acid substitutions caused by *CYP2E1*2* and *CYP2E1*3* affect the metabolism of benzene and toluene. To achieve this, CYP2E1 enzymes of wild-type (CYP2E1.1) and variants (CYP2E1.2, CYP2E1.3 and CYP2E1.4) were heterologously expressed in yeast cells, and the in vitro metabolism of benzene to phenol and toluene to benzyl alcohol was examined.

Materials and methods

Materials

pYES2/CT yeast expression vector was purchased from Invitrogen (Carlsbad, CA, USA); yeast nitrogen base was from BD Diagnostics (Franklin Lakes, NJ, USA); Zymolyase 100T was from Seikagaku Corporation (Tokyo, Japan); benzene, phenol, toluene, benzyl alcohol, *p*-methylbenzyl alcohol and 4-nitrophenol were from Nacalai Tesque (Kyoto, Japan); cytochrome c from horse heart and chlorzoxazone and 6-hydroxychlorzoxazone were from Sigma–Aldrich (St. Louis, MO, USA); $NADP^+$, glucose 6-phosphate and glucose 6-phosphate dehydrogenase were from Oriental Yeast (Tokyo, Japan); rabbit anti-human CYP2E1 antibody was from Novus Biologicals (Littleton, CO, USA); peroxidase-conjugated goat anti-rabbit immunoglobulin was from Zymed Laboratories (South San Francisco, CA, USA); and enhanced chemiluminescence-plus reagents were from GE Healthcare Bio-Sciences (Little Chalfont, UK). All other chemicals and reagents were of the highest quality commercially available.

Expression of CYP2E1 enzymes

CYP2E1*1A cDNA cloned into pGEM-T vector (pGEM-T/CYP2E1*1A) (Hanioka et al. 2007), wild-type CYP2E1 plasmid, was used as a template to generate point mutations in the target sites. The cDNAs of CYP2E1*2, CYP2E1*3 and CYP2E1*4 were constructed with a QuikChange site-directed mutagenesis kit according to the manufacturer's instructions using the primers listed in Table 1. All CYP2E1 plasmids were sequenced to confirm successful mutagenesis. The wild-type and variant CYP2E1 cDNAs were subsequently subcloned into the pYES2/CT yeast expression vector. The pYES2/CT vectors containing CYP2E1 cDNAs were used to transform INV*Sc*1/OR (Hanioka et al. 2007) by the lithium acetate procedure (Schiestl and Gietz 1989). The yeast transformants were cultivated, and the microsomal fractions were prepared as described previously by (Hanioka et al. 2007). The microsomes were stored at –80°C until used.

Assay for CYP2E1 holo- and apoproteins

Yeast cell microsomes were diluted to a protein concentration of 5.0 mg/mL with 100 mM potassium phosphate buffer (pH 7.4) containing 20% (v/v) glycerol and 0.4% (w/v) Emulgen 911, and total functional CYP contents